



1 **Drought-induced biomass burning as a source of black carbon to the Central**
2 **Himalaya since 1781 CE as reconstructed from the Dasuopu Ice Core.**

3

4 Joel D. Barker^{1,2}, Susan Kaspari³, Paolo Gabrielli^{1,2}, Anna Wegner², Emilie Beaudon²,
5 M. Roxana Sierra-Hernández², Lonnie Thompson^{1,2}

6

7 ¹ Byrd Polar and Climate Research Center, The Ohio State University, Columbus,
8 43210, USA.

9 ² School of Earth Sciences, The Ohio State University, Columbus, 43210, USA

10 ³ Department of Geological Sciences, Central Washington University, Ellensburg, USA,
11 98926

12

13 *Correspondence to:* Joel D. Barker (barke269@umn.edu)

14

15 **Abstract**

16 Himalayan glaciers are melting due to atmospheric warming with the potential to limit
17 access to water for more than 25% of the global population that reside in these glacier
18 meltwater catchments. Black carbon has been implicated as a factor that is contributing
19 to Himalayan glacier melt, but its sources and mechanisms of delivery to the Himalayas
20 remain controversial. Here, we provide a 211-year ice core record spanning 1781 –
21 1992 CE for refractory black carbon (rBC) deposition from the Dasuopu glacier ice core,
22 that has to date provided the highest elevation ice core record (7200 m). We report an
23 average rBC concentration of 1.5 µg/L (SD = 5.0, n = 1628) over the 211-year period.
24 An increase in the frequency and magnitude of rBC deposition occurs after 1877 CE,
25 accompanied by decreased snow accumulation associated with a shift in the North
26 Atlantic Oscillation Index to a positive phase. Typically, rBC is deposited onto Dasuopu
27 glacier during the non-monsoon season, and short-lived increases in rBC concentration
28 are associated with periods of drought within neighboring regions in north-west India,
29 Afghanistan and Pakistan. Using a combination of spectral and back trajectory
30 analyses, and comparison with a concurrent analysis of trace metals at equivalent
31 depths in the same ice core, we show that biomass burning resulting from dry



32 conditions is a source of rBC to the central Himalaya, and is responsible for deposition
33 that is up to 60 times higher than the average rBC concentration over the time period
34 analyzed. We suggest that biomass burning is a significant source of rBC to the central
35 Himalaya, and that the rBC record can be used to identify periods of drought in nearby
36 regions that are up-wind of Dasuopu glacier.

37

38 **1 Introduction**

39 Although the rate and extent of glacier melt differs geographically, the overall trend of
40 glacier mass loss globally, and particularly in mountain glaciers, is well documented
41 (IPCC, 2013). While warming summer temperatures resulting in increased glacier mass
42 loss and decreasing precipitation as snow are important factors contributing to glacier
43 mass wastage (Sakai and Fujita, 2017), the deposition of atmospheric aerosols that
44 darken the glacier surface also contribute to melt (Flanner et al., 2007; Xu et al., 2009).
45 The most efficient of these aerosols is black carbon (BC) which is produced by a variety
46 of combustion processes (Bond et al., 2004, 2013), most commonly by the incomplete
47 combustion of fossil fuels and biomass (Jacobson, 2004; Hammes et al., 2007). BC is
48 also the dominant absorber of visible light in the atmosphere (Lindberg et al., 1999) and
49 exerts a positive radiative forcing globally, second only to CO₂ (+1.1 W m⁻² and +1.6 W
50 m⁻² respectively; Ramanathan and Carmichael, 2008). BC continues to absorb radiation
51 upon deposition from the atmosphere onto glacier surfaces, reducing ice and snow
52 albedo, leading to melt (Hansen and Nazarenko, 2004; Forster and Ramaswamy, 2007;
53 Xu et al., 2009; Doherty et al., 2013).

54

55 A significant source of BC emitted to the atmosphere results from anthropogenic activity
56 (Ramanathan and Carmichael, 2008; Bond et al., 2013). The BC flux to the atmosphere
57 has increased by a factor of 2.5 since the European Industrial Revolution, resulting in an
58 increase of the global atmospheric BC burden by a factor of 2.5 - 3 (Lee et al., 2013).
59 BC's relatively short atmospheric residence time influences its distribution globally, with
60 the highest concentrations being proximal to BC emission sources (Bond et al., 2007;
61 Xu et al., 2009; Bond et al., 2013). Asian regions surrounding the Himalaya are major
62 sources of atmospheric BC (Novakov et al., 2003; Bond et al., 2007; Ramanathan et al.,



63 2007; Bond et al., 2013) and southern Himalayan glaciers are particularly influenced by
64 BC emissions from India (Kopacz et al., 2011; Gertler et al., 2016) and more local
65 emission sources that may add to the broader-scale regional flux (Kaspari et al., 2011).
66
67 Atmospheric aerosols, including BC, are warming the cryosphere and accelerating snow
68 melt in the western Tibetan Plateau and Himalayas (Lau et al., 2010) and altering the
69 regional hydrologic cycle (Immerzeel et al., 2010). This is a concern because Hindu
70 Kush Himalayan (HKH) glacier melt affects the water security, particularly during the
71 early- and post-monsoon season (Hill et al., 2020), of densely populated regions of
72 south-east Asia. Meltwater from HKH glaciers are the source of ten major rivers that
73 provide water for irrigation, hydropower, and ecosystem services for two billion people
74 across Asia (Scott et al., 2019); over 25% of the global population.
75
76 Research into BC's interaction with the HKH cryosphere has increased in recent years.
77 Several studies have documented the magnitude and timing of BC deposition using
78 short-term BC records preserved in surface snow that span 1 - 2 years (e.g. Xu et al.,
79 2009; Ming et al., 2008; Ming et al., 2012; Kaspari et al., 2014; Zhang et al., 2018; Thind
80 et al., 2019). More recently, continuous surface measurements of near-surface
81 aerosols, including BC, have been reported for the HKH region (e.g. Marinoni et al.,
82 2010; Bonasoni et al., 2010; Cao et al., 2010; Babu et al., 2011; Chaubey et al., 2011;
83 Marinoni et al., 2013; Niu et al., 2017; Negi et al., 2019). While useful for tracking the
84 evolution of atmospheric BC at high temporal resolution, these studies do not provide a
85 longer-term historical context against which current levels of BC can be compared.
86 Records of BC deposition preserved in ice cores are useful as longer-term
87 environmental archives for reconstructing atmospheric aerosol composition that span
88 decades (Liu et al., 2008; Ming et al., 2008; Ginot et al., 2014). In the HKH region, these
89 archives are essential for identifying trends in BC deposition onto HKH glaciers in
90 response to increasing BC emissions in surrounding regions. For example, Ming et al.
91 (2008) report an increasing trend in BC deposition onto East Rongbuk Glacier (Mt.
92 Everest; 6500 m above sea level (asl)) during a 10 year period beginning in 1965, and
93 then another increase beginning in 1995 to the end of the record in 2001. Xu et al.



94 (2009) report a period of relatively high concentrations in the 1950s and 1960s in 4
95 Himalayan and Tibetan Plateau glaciers (Muztagh Ata, Guoqu glacier, Noijin Kangsang
96 glacier, East Rongbuk glacier, and Tanggula glacier) and suggest a European source of
97 BC to these sites. They also note an increase in BC on the eastern-most site (Zuoqiupu
98 glacier) beginning in the 1990s and suggest an Indian source of BC for the region.
99 Similarly, Liu et al. (2008) report high elemental carbon (a form of BC) at Muztagh Ata
100 from 1955 - 1965. Ginot et al. (2014) report BC concentrations at Mera Glacier from
101 1999 - 2010, and suggest that variations in BC over this period respond primarily to
102 monsoonal rather than anthropogenic forcing.

103

104 Kaspari et al. (2011) were the first to present a BC record that extended back to the pre-
105 industrial period (1860-2000) in an ice core from East Rongbuk glacier (6518 m asl) and
106 reported a threefold increase in BC deposition since 1975, indicating that anthropogenic
107 BC is contributing to the BC flux to the southern Himalaya. Jenkins et al. (2016) report
108 an increase in BC deposition in the central Tibetan Plateau beginning in 1975 from the
109 Guoqu glacier ice core record spanning 1843-1982. These deep ice core records are
110 valuable for evaluating long-term trends in BC spanning the Industrial Revolution to the
111 present and the concomitant increase in anthropogenically-sourced BC emissions.
112 Additional ice core-derived BC records that span the period of industrialization in Asia
113 are required to both corroborate existing historical records of BC deposition onto HKH
114 glaciers and to establish a regional baseline record for BC fluxes onto the region. These
115 records are currently lacking for the HKH and are essential for identifying regional-scale
116 trends in BC deposition.

117

118 The highest elevation ice core record ever obtained is the Dasuopu ice core (C3;
119 Thompson et al., 2000), which was retrieved from the Dasuopu Glacier in the Central
120 Himalaya (28.38 °N, 85.72 °E; Fig. 1) in 1997 at an elevation of 7200 m asl. Thompson
121 et al. (2000) determined that monsoonal precipitation is responsible for the net
122 accumulation of snow onto the glacier surface, in the order of 1000 mm water
123 equivalent per year (in 1996), permitting an annually resolved environmental record
124 spanning 1440 - 1997 CE (Thompson et al., 2000). The remote location and high



125 elevation of the Dasuopu ice core drill site suggests that any local influence on the
126 deposition of atmospheric aerosols onto the glacier surface is minimal, and that
127 accumulation is representative of mixed free tropospheric composition (Kumar et al.,
128 2015). Evidence suggesting that the Dasuopu glacier differs from lower-elevation
129 glaciers in the region with respect to seasonal meteorology supports the hypothesis that
130 the flux of aerosols onto the glacier surface may be more representative of free
131 tropospheric composition rather than being affected by local (valley-scale)
132 meteorological conditions (Li et al, 2011).

133

134 Here, we quantify refractory BC (rBC; a subset of the broader BC descriptor of
135 carbonaceous particles that it is measured by laser induced incandescence specifically;
136 Lack et al., 2014) in a section of the Dasuopu ice core from 1781-1992 CE at annual to
137 sub-annual resolution in the glacier ice portion. We employ spectral analysis of the rBC
138 ice core time series to identify trends in rBC deposited onto Dasuopu glacier across
139 several temporal scales and to avoid “peak-picking” that might lead to subjectively
140 identifying episodes of increased rBC in the ice core time series. The rBC record is
141 compared to trace-element analysis of samples from equivalent depths along the same
142 ice core, as described by Gabrielli et al. (2020), and an atmospheric back trajectory
143 analysis to elucidate the broader-scale trends of deposition and potential rBC sources to
144 the southern Himalaya.

145

146 **2 Methods**

147 **2.1 The Dasuopu Ice Core**

148 Dasuopu glacier descends to the north from Mt. Xixiabangma in the Central Himalaya
149 (Fig. 1). The ice core examined here was drilled from the Dasuopu glacier surface to
150 bedrock (145.4 m) with an electromechanical drill, without using drilling fluid, and
151 provides a continuous record of deposition onto the glacier surface from 1010 to 1997
152 CE (Thompson et al. 2000). Here, we examine the upper section of the C3 ice core
153 (hereafter referred to as the “Dasuopu core”), from 8.4 - 120.3 m depth from the
154 surface, corresponding to the period 1781 - 1992 CE. Sections of the Dasuopu core
155 outside of this interval were not available for analysis. We use the Thompson et al.



156 (2000) chronology that was established using $\delta^{18}\text{O}$, dust, and NO_3^- measurements, as
157 well as annual layer counting confirmation using the location of the 1963 CE beta
158 radioactivity peak from thermonuclear tests at a depth of 42.2 m to determine the core's
159 age-depth relationship. Thompson et al. (2000) also used two major monsoon failures
160 (1790-1796 and 1876-1877) as age/depth benchmarks that are reflected in the dust and
161 Cl^- records to validate the ice core dating chronology. The chronology is accurate to ± 3
162 years (Thompson et al., 2000).

163

164 **2.2 Sample Preparation**

165 A portion of the Dasuopu core has been housed in the Ice Core Storage Facility (Byrd
166 Polar and Climate Research Center (BPCRC)) at $-30\text{ }^\circ\text{C}$ since the original analysis by
167 Thompson et al. (2000). The portion of the Dasuopu core analyzed here is
168 characterized by consolidated firn from 8.4 m - 56.4 m and glacier ice from 56.4 - 120.3
169 m depth. Ice was sampled continuously (with the exception of intervals noted in Suppl.
170 Info. Table 1) in a cold room ($-5\text{ }^\circ\text{C}$) at sub-annual resolution (2.5 - 10 cm sample
171 interval) with a band saw along the length of the ice section. Each ice sample was
172 divided in half to permit the analysis of BC and trace elements from identical depths
173 throughout the core ($n = 1572$). Prior to rBC analysis, each ice sample was rinsed with
174 MQ water at room temperature in a class 100 laboratory to remove any contaminants
175 from the outer edges of the core, placed in a sealable polyethylene bag and
176 immediately stored frozen ($-34\text{ }^\circ\text{C}$) to ensure that the sample did not melt prior to
177 analysis.

178

179 Due to sample volume limitations resulting from previous studies of the Dasuopu core
180 (e.g. Thompson et al., 2000; Davis et al., 2005), 56 firn samples (5.5 - 10 cm length)
181 were collected at discontinuous intervals (where sufficient sample volume was
182 available) from 8.4 - 56.4 m depth in the cold room ($-5\text{ }^\circ\text{C}$) using a band saw. The outer
183 2 cm of each sample ($n = 56$) was removed using clean stainless-steel knives (soaked
184 in HNO_3^- and rinsed with MQ water) under laminar flow conditions in the cold room to
185 remove surface contaminants. Clean firn samples were stored frozen ($-30\text{ }^\circ\text{C}$) in double
186 Ziploc bags until analysis.



187

188 **2.3 BC analysis**

189 rBC was quantified by laser induced incandescence using a Single Particle Soot
190 Photometer (SP2; Droplet Measurement Technologies, Longmont, U.S.A.; Schwarz et
191 al., 2006; Wendl et al., 2014) at Central Washington University (Ellensburg, WA, USA).
192 Frozen samples were melted at room temperature, transferred from storage bags into
193 50 ml polypropylene centrifuge tubes, and sonicated for 20 minutes immediately prior to
194 analysis. Each liquid sample was stirred with a magnetic bar as water was routed into a
195 CETAC U-5000AT+ ultrasonic nebulizer (Teledyne CETAC Technologies, Omaha,
196 U.S.A.) using a peristaltic pump. The resultant aerosols flowed to the SP2 inlet at a
197 known rate using carbon-free air carrier gas. The peak intensity of light emitted by an
198 incandescing rBC particle is linearly proportional to its mass (Schwarz et al., 2006), and
199 the SP2 detects this emitted light using the amplified output from 2 photodetectors
200 (broadband and narrowband) to provide a detection range of ~70 – 500 nm volume-
201 equivalent-diameter (VED; Kaspari et al., 2014). A 5-point calibration curve using
202 Aquadag standards and MQ water was performed daily to correct for BC loss during
203 nebulization (Wendl et al., 2014). MQ water was analyzed every 5 samples as a blank
204 to monitor instrument baseline conditions. If the baseline was above background levels,
205 then MQ water would be run through the system until stability was achieved. Baseline
206 instability was not observed throughout the course of the analysis. The SP2 data output
207 was processed using the PSI SP2 Toolkit ver. 4.100a (Paul Scherrer Institut, CH) and
208 the IGOR Pro software platform (WaveMetrics Inc., Portland, U.S.A.).

209

210 **2.4 Spectral analysis**

211 The record of rBC concentration with depth through the Dasuopu ice core provides a
212 time series of rBC deposition onto Dasuopu glacier over time. The decomposition of the
213 time series into time-frequency space using spectral analysis (wavelet analysis) permits
214 the identification of dominant modes of variability and their variance with time (Torrence
215 and Compo, 1998). Wavelet analysis is well suited to the analysis of time series data
216 where frequency and/or magnitude is non-stationary through the signal (Debret et al.,
217 2007). For example, wavelet analyses have been used to identify Himalayan climatic



218 oscillations related to orbital forcing, Dansgaard-Oeschger cycles, and Heinrich events
219 in the 1992 Guliya ice core (Yang et al., 2006), characterize the increased role of ENSO
220 climate forcing on Antarctic temperature since ~1850 from ice core records from East
221 and West Antarctica (Rahaman et al., 2019), and a switch from external forcing to
222 internal forcing mechanisms on global climate during the mid-Holocene (Debret et al.,
223 2009).

224

225 The ice core sampling strategy employed here may influence the results of the spectral
226 analysis because the uppermost firn section was not sampled continuously and there
227 are occasional sampling gaps in the glacier ice section (Suppl. Info. Table 1). The
228 discontinuous sampling of the firn section likely resulted in an incomplete
229 characterization of rBC deposition onto the Dasuopu glacier since 1944 (56.4 m depth).
230 Further, the number of samples per year is not consistent throughout the record
231 because of interannual differences in snow accumulation (Suppl. Info. Fig. 1). It is
232 important to note that the spectral analysis treats the rBC time series as a linear depth-
233 time function. However, because the depth-time relationship in the ice core is not linear,
234 data is treated here as a function of the sample number of progression with depth in the
235 ice core, while the dates of the individual features detected relative to sample number
236 are specified using the Thompson et al. (2000) depth-age model. Therefore, the
237 spectral decomposition of the time series into time-frequency space is achieved while
238 minimizing the influence of data gaps and non-linear accumulation rate.

239

240 The wavelet analysis of the Dasuopu rBC record was performed using the Wavelet
241 Toolbox in Matlab (ver. R2020a; Mathworks). A continuous 1-D wavelet transform was
242 generated to identify modes of variability and the characteristics of that variability with
243 time throughout the rBC record. The Mexican Hat (or Rickler) mother wavelet was
244 chosen because it is similar to the shape of the annual variability in the rBC
245 concentration signal across the time series (Suppl. Info. Fig. 2).

246

247

248 **2.5 Trace element analysis**



249 Trace element quantification at equivalent depths as the rBC was only possible for the
250 glacier ice section of the Dasuopu ice core due to lack of sampling volume in the
251 corresponding overlying firn sections. Trace element concentration was determined by
252 Inductively Coupled Plasma Sector Field Mass Spectrometry (ICP-SFMS) at BPCRC.
253 Twenty three trace elements were measured (Al, As, Ba, Bi, Cd, Co, Cr, Cs, Fe, Ga,
254 Mg, Mn, Mo, Nb, Ni, Pb, Rb, Sb, Ti, Tl, U, V, and Zn) using methods described in
255 Uglietti et al. (2014). The trace element crustal enrichment factor (EF) is used to identify
256 trace element contributions exceeding natural background levels, and was calculated
257 relative to Fe and elemental ratios of dust from the Tibetan Plateau following Gabrielli et
258 al. (2020) as an additional variable to be compared with rBC.

259

260 **2.6 Back trajectory analysis**

261 While the complex geomorphology of the Himalayas affects local wind patterns, back
262 trajectory modeling permits the characterization of the broader regional catchment from
263 which rBC may be derived. Atmospheric circulation capable of delivering rBC to
264 Dasuopu glacier was identified using the Hybrid Single Particle Lagrangian Trajectory
265 Model (HSYPLIT; NOAA Air Resources Laboratory, 2018). A 7-day back trajectory was
266 chosen as a conservative estimate of rBC atmospheric residence time given the range
267 reported in the literature (e.g. Ogren and Charlson, 1983; Reddy and Boucher, 2004,
268 2007; Samset et al., 2014; Lund et al., 2018). Back trajectories from the Dasuopu drill
269 site were calculated at 6 hour intervals from 1948-1991 for January (winter/non-
270 monsoon) and July (summer/monsoon) using the NCEP/NCAR (National Centers for
271 Environmental Prediction/National Center for Atmospheric Research) reanalysis from
272 1948 (the limit of the NCEP/NCAR dataset) to 1991.

273

274 **3 Results**

275 **3.1 The rBC record**

276 Figure 2a shows the 211-year rBC record from the Dasuopu ice core. The mean rBC
277 concentration is 1.5 $\mu\text{g/L}$ ($SD = 5.0$, $n = 1628$) from 1781 (± 3 years) to 1992 CE. The
278 mean rBC concentration in the glacier ice section from 1781 to 1944 and the
279 discontinuously sampled firn section from 1944 to 1992 is 1.4 $\mu\text{g/L}$ ($SD = 4.4$, $n = 1572$)



280 and 6.0 $\mu\text{g/L}$ (SD = 13.2, $n = 56$), respectively. Note that the median values for the
281 same time periods are less influenced by outliers with high concentrations (median
282 1781 to 1944 = 0.2 $\mu\text{g/L}$, 1944 to 1992 = 0.6 $\mu\text{g/L}$). Even though the rBC concentration
283 in the ice and firn described here is significantly different (two tailed Mann-Whitney U
284 test, $p < 0.05$), the effect of discontinuously sampling the firn section and its accurate
285 characterization of rBC since 1944 is unknown. It is possible that the firn section is
286 biased towards higher rBC concentrations because only 26% (14 of 54) of the firn
287 samples correspond to snow deposited during monsoon conditions, as indicated by
288 depleted $\delta^{18}\text{O}$ (data not shown), that is a period associated with lower atmospheric
289 aerosol loading (Lelieveld et al., 2018). In general, rBC deposition corresponds to $\delta^{18}\text{O}$
290 enrichment (Fig. 3) and increased dust in glacier ice, indicating that rBC is deposited
291 during the non-monsoonal dry season (Fig. 3; Kaspari et al., 2014). Occasional
292 exceptions occur, for example in 1824 CE, when a period of high rBC deposition
293 corresponds to a relatively low dust concentration and a low $\delta^{18}\text{O}$ value (Fig. 3a).

294

295 The smoothed (5 year median) rBC concentration and flux (the product of mean annual
296 rBC concentration and snow accumulation) records show an increase beginning in
297 ~ 1870 and again in ~ 1940 (Fig. 2a, b). The discontinuous firn section of the core has
298 elevated concentrations during the late 1960s - 1970s, consistent with observations
299 from East Rongbuk glacier by Ming et al. (2008) and Kaspari et al. (2011), and for
300 Tanggula glacier by Xu et al. (2009).

301

302 **3.2 Spectral Analysis**

303 The spectral analysis of the rBC record identifies three modes of variability (Fig. 4b):

304 First, the mode at $a = 6$ ($a = 0.5 \times \text{frequency}$) indicates high frequency, and
305 generally, relatively low amplitude variability in spectral coefficients (81% of rBC
306 concentrations are $< 1 \mu\text{g/L}$) occurring at \sim annual (12 data points/year; SD = 4.3, $n =$
307 112) resolution with isolated relatively higher amplitude events dispersed throughout the
308 record (Fig. 4c). The frequency of these higher amplitude events increases from ~ 1877
309 until 1992 CE (Fig. 4a, c).



310 Second, a lower frequency mode ($a = 27$; ~ 4.5 years) captures periodic peaks in
311 rBC concentrations centered at 1825, 1877, 1888, 1908, 1920, 1930, and 1977 CE if
312 peaks that are $>25\%$ of the largest peak's amplitude in the time series (1977 CE) are
313 considered (Fig. 4d). Dips in the $a = 27$ spectral coefficients indicating periods of low
314 amplitude (defined here as $>25\%$ of the amplitude of the lowest dip at 1937 CE), occur
315 at 1818, 1868, 1875, 1880 - 1884, 1893, 1914, 1924, and 1937 CE (Fig. 4d).

316 Third, the $a = 512$ (~ 85 year) mode identifies a shift from samples with negative
317 spectral coefficients to those with positive spectral coefficients at 1877 CE (Fig. 4e). All
318 three modes identify a period early in the rBC record characterized as a quiescent
319 period (1781 - 1877 CE) where rBC concentrations do not exceed $19.3 \mu\text{g/L}$ (mean =
320 0.8 , $\text{SD} = 3.0$, $n = 880$), except for the isolated peak ($63.3 \mu\text{g/L}$) at 1825 CE (Fig. 4a, c,
321 d)). Prior to 1877 the rBC concentration in the ice core is significantly lower (Mann-
322 Whitney U test, $p < 0.05$) and less variable (mean = 0.8 , $\text{SD} = 3.03$, $n = 898$) than the
323 post 1877 period (mean = 2.3 , $\text{SD} = 6.6$, $n = 732$; Fig. 4). While the ~ 85 year mode
324 identifies a shift from negative to positive spectral coefficients in 1877, the 5 year
325 median of the rBC record identifies an increase occurring at ~ 1870 . This suggests that
326 the wavelet analysis may be sensitive to individual or tightly clustered peaks in the rBC
327 record, such as those that occur between 1875 and 1880 (Fig. 3a, 4a).

328

329 **3.3 Comparison of the rBC record with the trace element record**

330 When considering the full record ($n = 857$ to 916 depending on the element; Table 1), all
331 of the trace element concentrations analyzed are significantly correlated with rBC
332 (range of 0.15 (Zn; $n = 915$) to 0.27 (Rb; $n = 914$); Table 1; $\alpha = 0.01$; Spearman
333 correlation test is used instead of Pearson correlation test because the rBC and trace
334 element data are not normally distributed). If the low-rBC pre-1877 period, as indicated
335 by the spectral analysis, is considered independently, then the correlation between
336 trace element and rBC are still statistically correlated (range of 0.26 (Zn, $n = 915$) to
337 0.44 (Mg and Mn, $n = 915$). In contrast, the post 1877 period shows a statistically
338 insignificant slightly negative correlation between the trace elements and rBC ranging
339 from -0.04 (Cs and Nb, $n = 913$ and 915 , respectively) to -0.10 (Bi and Mn, $n = 857$ and
340 915 , respectively).



341

342 The crustal enrichment factor (EF) for all of the trace elements were significantly weakly
343 to moderately negatively correlated with rBC for all trace elements, ranging from -0.21
344 for Mg to -0.57 for Ga, except for Mn which was insignificantly positively correlated
345 (0.02). The trace element EFs were more negatively correlated to rBC during the post
346 1877 period than the pre-1877 period (excluding Mn because it was insignificantly
347 correlated; SD = 0.14), although this difference is not statistically significant, $t(22) =$
348 1.88, $p = 0.07$ ($p < 0.05$).

349

350 **3.4 Back trajectory**

351 Figure 5a shows the results of the July back trajectory showing that aerosols are
352 primarily derived from areas to the south-west of the Dasuopu drill site, from the Arabian
353 Sea and across western and northern India during the monsoon. A secondary source is
354 located to the west and draws atmospheric aerosols from the eastern Mediterranean
355 Sea and Arabian Peninsula. January (non-monsoon) circulation is derived from the
356 westerly circulation across north-eastern Africa, Central Europe, the Arabian Peninsula
357 and north-west India (Fig. 5b).

358

359 **4 Discussion**

360 **4.1 rBC concentrations**

361 The mean rBC concentration in the Dasuopu ice core, from 1781 to 1992 CE is 1.5 $\mu\text{g/L}$
362 (SD=5.0, n=1628); 6 times higher than the average rBC reported by Kaspari et al.
363 (2011) for the period 1860-1992 and ~2 times lower than BC reported by Ming et al.
364 (2008) and Xu et al. (2008) for the East Rongbuk ice core record over similar time
365 periods (Fig. 1). Note that while Kaspari et al. (2011) measured BC from the East
366 Rongbuk core using the same incandescence method used here, samples were stored
367 as liquid and measured concentrations are likely underestimated due to rBC particle
368 adherence onto the walls of the storage container and/or agglomeration of BC particles
369 above the detected particle size range (Wendl et al., 2014; Kaspari et al., 2014). In
370 contrast, Ming et al. (2008) and Xu et al. (2009) measured BC concentration by thermo-
371 optical methods, which may result in an overestimation of reported BC due to organic



372 matter pyrolysis during analysis (Gilardoni and Fuzzi, 2017), and a larger fraction of the
373 carbonaceous particles being classified as BC.

374

375 **4.2 rBC seasonality**

376 Seasonally, peaks in rBC concentration correspond to intervals of increased dust
377 concentration and enriched $\delta^{18}\text{O}$ over the entire ice core record (see examples in Fig.
378 3), indicating most BC deposition occurs during the non-monsoonal season when drier
379 westerly air masses dominate atmospheric circulation (Fig. 5). Weather station
380 measurements and previous snow/ice studies in the region confirm that rBC
381 concentrations are lower in near-surface air at the Nepal Climate Observatory-Pyramid
382 (NCO-P; 5079 m a.s.l.) during the monsoon (Bonasoni et al., 2010; Marinoni et al.,
383 2010, 2013) and higher during the pre-monsoon period (Babu et al., 2011; Nair et al.,
384 2013; Ginot et al., 2014; Kaspari et al., 2014; Chen et al., 2018).

385

386 **4.3 Temporal variations in rBC deposition and regional climate**

387 The pre-1877 CE period differs from the post-1877 CE period in the frequency and
388 amplitude of variability in rBC deposition (Fig. 2a and 4e). The high BC deposition event
389 in ~1825 CE (Fig. 4c) occurs during an otherwise quiescent pre-1877 CE period
390 coinciding with a time of severe regional moisture stress/droughts as reflected in
391 suppressed tree ring growth across Nepal, peaking in 1817 CE (Figs. 6 and 7 in Thapa
392 et al., 2017). This period of abnormally dry conditions occurs after 2 large volcanic
393 events; the Tambora eruption of 1815 (Stothers, 1984) and an eruption of unknown
394 origin in 1809 CE (Cole-Dai et al., 2009). Anchukaitis et al. (2010) argue that major
395 explosive eruptions in the tropics can disrupt the Asian monsoon system and result in
396 drier conditions in central Asia for up to 8 years afterward. Dry conditions are typically
397 associated with an increase in the frequency and severity of biomass burning in south-
398 east Asia (Baker and Bunyavejchewin, 2009) and the association between dry
399 conditions and increases in rBC deposition suggests that biomass burning may be a
400 source of high rBC deposition events onto Dasuopu glacier.

401



402 From ~1877 CE until the end of the rBC record in 1992, rBC concentrations are
403 significantly higher and the amplitude of rBC deposition increases, as indicated by the
404 shift from negative to positive spectral coefficients at $a = 512$ (Fig. 4e). This suggests a
405 change in either the magnitude of rBC emission source(s) or in the atmospheric
406 mechanism that delivers rBC to Dasuopu glacier after ~1877 CE. The post ~1877
407 increase in rBC corresponds to a decrease in snow accumulation onto Dasuopu glacier
408 (Fig. 2c; Davis et al., 2005) and an increase in the rBC flux from the atmosphere
409 beginning in ~1880 (Fig. 2b). This decrease in snow accumulation has been linked to a
410 strengthening of the Icelandic Low pressure system as temperatures in the Northern
411 Hemisphere warmed at the termination of the Little Ice Age (LIA). This resulted in a shift
412 in the North Atlantic Oscillation Index (NAO) from a negative mode to a positive mode,
413 contributing less moisture to the southern Himalaya during winter (Davis et al., 2005).
414 Less winter snow accumulation post ~1877 would be associated with drier winter (non-
415 monsoon) conditions generally, when rBC deposition onto Dasuopu glacier is highest.
416

417 **4.4 The influence of drought and biomass burning on the rBC record**

418 Biomass burning, and associated rBC emissions result from dry conditions and drought
419 that lowers the water table and dries biomass fuel (Baker and Bunyavejchewin, 2009;
420 Tosca et al., 2010). Further, aerosols produced during fires may contribute to a positive
421 feedback cycle where smoke plume shading decreases sea surface temperature, while
422 increased concentrations of atmospheric BC warm and stabilize the troposphere,
423 suppressing convection and precipitation and intensifying drought conditions on land
424 (Tosca et al., 2010). High BC aerosol levels in ambient air corresponding to agricultural
425 burning beginning in late April and forest fire activity during the non-monsoon season
426 was reported by Negi and others (2019) from ambient air measurements at Chirbasa,
427 India (Gangotri glacier valley) during 2016. The spectral coefficients calculated here
428 identify trends in rBC deposition onto Dasuopu glacier and can be compared to regional
429 rainfall data from a network of rain gauge stations that are distributed across India to
430 identify periods of dryness (e.g., Parthasarathy et al. 1987) associated with rBC
431 deposition.
432



433 Continuous regional instrumental rainfall records within the atmospheric catchment for
434 atmospheric aerosols to Dasuopu glacier prior to the early 1900s CE are rare, and
435 biomass burning records are non-existent. However, continuous tree ring-based
436 reconstructions of precipitation conditions for Europe, North Africa, and the Middle East
437 is provided by the Old World Drought Atlas (OWDA; Cook et al., 2015) and includes
438 areas identified by the back trajectory analysis as being potential source regions for rBC
439 to Dasuopu glacier (Fig. 5b). The Monsoon Asia Drought Atlas (MADA; Cook et al.,
440 2010) provides a similar dataset for regions in East Asia, including Pakistan and
441 Afghanistan, which may contribute rBC to Dasuopu glacier (Fig. 5b). An instrumental
442 record for both the OWDA and MADA begins in 1901 (Fig. 6). Comparing the peaks in
443 rBC deposition identified by the spectral coefficients ($a = 27$, ~ 4.5 year frequency)
444 centered at 1825, 1877, 1888, 1898, 1908, 1920, 1930, and 1977 CE (Fig. 4d) to the
445 reconstructed and instrumental self-calibrating Palmer Drought Severity Index (scPDSI)
446 for the summer season (where positive and negative scPDSI indicate wet and dry
447 conditions respectively; Fig. 6), it is possible to identify periods of dryness that might
448 contribute to the production of rBC by biomass burning.

449
450 rBC wavelet coefficient peaks in 1825 and 1877 CE occur at the end of a decade-long
451 period of negative scPDSI in the OWDA and MADA reconstructions, respectively (Fig.
452 6). Similarly, 1888, 1898, and 1930 follow years of negative scPDSI in either the OWDA
453 or MADA reconstructions, indicating periods of dryness preceding episodes of rBC
454 deposition onto Dasuopu glacier (Fig. 6). The 1908 and 1920 CE peaks do not follow
455 periods of negative scPDSI in the OWDA or MADA reconstructions, but follows periods
456 of negative scPDSI in the MADA instrumental record (Fig. 6) indicating that dryness is
457 associated with these rBC deposition peaks as well. The peak centered at 1977 CE
458 follows periods of positive scPDSI in the OWDA and MADA reconstructions and
459 instrumental records and does not appear to be related to abnormally dry conditions,
460 and may indicate an unidentified source of rBC. Conversely, dips in the spectral
461 coefficients at a ~ 4.5 year frequency ($a = 27$) indicate periods of low rBC deposition
462 occurring at 1818, 1868, 1875, 1880-1884, 1893, 1914, 1924, and 1936 CE. With the
463 exception of the dip centered at 1875 and 1936 CE, dips in the spectral coefficient



464 record follow periods of positive scPDSI in either or both the OWDA and MADA tree ring
465 reconstruction. While dips centered at 1914 and 1924 CE follow periods of positive
466 scPDSI in both the OWDA and MADA instrumental record, 1936 CE follows a period of
467 positive scPDSI in the MADA instrumental record only (Fig. 6).

468

469 In addition to the scPDSI from OWDA and MADA tree ring reconstructions and the
470 instrumental record (since 1900 CE), an independent historical record for rainfall is
471 available for India that was compiled by Mooley et al. (1981) and has since been
472 reported in terms of drought/flood severity by Parthasarathy et al. (1987; Suppl. Table
473 1a, b). As mentioned, several periods of high rBC concentration are identified by the
474 spectral coefficients at $a = 27$ (~4.5 year frequency) centered at 1825, 1877, 1888,
475 1898, 1908, 1920, 1930, and 1977 CE (Fig. 4d). These periods of high rBC deposition
476 coincide with periods of drought reported for India, particularly in western/northwestern
477 meteorological subdivisions (Parthasarathy et al., 1987) within the ± 3 years dating error
478 of the ice core chronology (Fig. 7; Suppl. Fig. 3 a). For example, from 1876 – 1878,
479 India experienced widespread moderate to severe drought conditions (Parthasarathy et
480 al., 1987; Fig. 7a) and soil moisture deficits (Mishra et al., 2019) that resulted in the
481 “Madras Famine” (Cook et al., 2010; Mishra et al., 2019). In 1888 (and 1891 which is
482 within the ± 3 year ice core dating uncertainty), regions in western and northwestern
483 India experienced moderate and severe drought conditions (Fig. 7b). In 1899
484 (corresponding to 1898 in the rBC record, ± 3 years), northwest and western
485 meteorological subdivisions (among others) experienced severe drought while
486 moderate drought was experienced by most of India (Fig. 7c), resulting in famine that
487 affected 59.5 million people (Mishra et al., 2019). In 1911 (1908 ± 3 years) there was
488 extreme drought reported in the northwest and moderate drought reported in the north-
489 central and southwest meteorological districts (Fig. 7d). In 1918 (1920 ± 3 years), there
490 was severe drought reported in the north and central-west and moderate drought
491 reported throughout the south and north-central regions of the continent (Fig. 7e). From
492 1927-1929 (1930 ± 3 years), moderate drought was reported in the northern region of
493 India (Fig. 7f). Similar to observations from the OWDA and MADA comparisons, the
494 ~1977 period does not stand out in the climate record as being exceptional (Suppl. Fig.



3), and it does not correspond to anomalously high rBC values (Fig. 2a) yet it corresponds with a period of highly positive spectral coefficients (Fig. 4c, d). Finite-length signal border effects (so called edge effects) have been well documented, where a wavelet transform (such as that used here) yield abnormal coefficients as the wavelet extends into the “shoulder areas” of the record that don’t have data (Su et al., 2011, Montanari et al., 2015). It is possible that the peak identified here at $a = 6$ and $a = 27$ is a result of wavelet transform edge effects. Alternatively, sources other than biomass burning, that have not been identified here, may contribute to high rBC values observed in the Dasuopu ice core ~1977 CE.

504

Dips in the $a = 27$ spectral coefficient record correspond to periods of flooding in India. For example, the trough at 1875 CE corresponds to reports of extreme flooding in the north-west and moderate flooding in western India (Fig. 8a). It should be noted that moderate drought was reported in the far west and south, but these conditions did not result in a rBC peak in the $a = 27$ coefficients (Fig. 4d). For the period ~1880 to 1886 CE, severe and moderate flooding is reported in the west in 1884 CE, with moderate drought to the south and east that did not result in an rBC peak in the $a = 27$ coefficients (Fig. 8b). From 1880 – 1882 CE, the continent experienced relatively stable conditions with moderate flooding in some western and north-western districts (Suppl. Info. Fig. 3). Western India experienced severe and moderate flooding in the west and northwest in 1893 (Fig. 8c), corresponding to a dip in the $a = 27$ coefficients (Fig. 4d). 1914 and 1917 (1914 ± 3 years), 1926 (1924 ± 3 years) and 1933 (1936 ± 3 years) all saw severe and/or moderate flooding in western meteorological districts, with no drought conditions reported in the rest of India, corresponding to dips in the $a = 27$ coefficients (Fig. 8d, e, f respectively).

520

521 **4.5 rBC and trace metals**

Recent work by Gabrielli and others (2020) suggested that atmospheric trace metals preserved in the Dasuopu ice core, likely linked to the long-range transport of fine fly ash, were indicative of emissions from coal combustion and fires used to clear forested areas to the west of the Himalayas since the beginning of the Industrial Revolution



526 (~1780 CE). Fly ash is composed of alumino-silicate and iron-rich byproducts of coal
527 combustion and biomass burning and is enriched in trace metals (Ross et al., 2002). Fly
528 ash is not detected by the SP2 as configured here.

529

530 We observe a general negative correlation between BC and the crustal enrichment
531 factor (EF; indicative of element concentrations above the natural background derived
532 from crustal material) of trace metals in the Dasuopu core, particularly after 1877 CE
533 (Table 1) when rBC spectral coefficients are positive at $\lambda = 512$ (Fig. 4e). This illustrates
534 that the deposition of the non-crustal fraction of trace metals (as indicated by a positive
535 EF), and fly ash, occurred out of phase from rBC.

536

537 rBC deposition resulting from biomass burning may be expected to correlate with trace
538 elements associated with the biomass source material (K, Cl, Zn, and Br; Echalar et al.,
539 1995). Of these, only Zn was analyzed here. Zn concentration is only weakly correlated
540 with rBC (0.15), although more strongly (0.26) in the pre-1877 period than in the post-
541 1877 period (-0.06), and Zn's EF is moderately negatively correlated, particularly in the
542 post 1877 period (-0.63). While the lack of correlation between potential biomass
543 burning-derived trace elements such as Zn and rBC might suggest a non-biomass
544 burning source for rBC, one should be cautious in attributing specific trace elements to
545 biomass burning events. For example, trace elements emitted during partial combustion
546 can vary depending on fire intensity (flaming vs. smoldering), fuel source (savanna vs.
547 forest) (Echalar et al., 1995), and size-dependent particle adhesion (Samsonov et al.,
548 2012). Further, biomass burning remobilizes soil-derived particles which would lower
549 the individual trace element's EF (Gaudichet et al., 1995) causing a negative correlation
550 between rBC and EF_c. There is a statistically significant negative correlation with rBC to
551 all of the trace EFs (except for Mn), suggesting that rBC deposition is not associated
552 with non-crustal trace element deposition, interpreted as an indicator of fly ash
553 deposition (Gabrielli et al., 2020), that is enriched above the natural dust input. Of
554 importance is that the discontinuous sampling of firn in the Dasuopu ice core record
555 presented here does not capture a continuous record of rBC deposition during the post



556 1970s; a period when rBC is reported to have increased in the southern Himalaya
557 (Kaspari et al., 2011) and Tibetan Plateau (Jenkins et al., 2016; Wang et al., 2015).
558

559 **5 Conclusions**

560 Here, we present the highest elevation (7200 m asl) record of rBC deposition ever
561 reported. This record is unique in its high elevation and represents conditions in the free
562 troposphere, away from local sources of BC. The Dasuopu record also contributes to
563 the limited number of proxy records of BC deposition in the HKH region where glacier
564 melt, and therefore factors such as BC that affect glacier melt, influence the water
565 security of one of the most densely populated regions of the planet. While the Dasuopu
566 rBC record presented here is not well resolved during the period after the 1970s, the
567 record does indicate elevated BC during 1970-1980, consistent with the Everest ice
568 core BC record that showed elevated BC post 1970 (Kaspari et al., 2011).

569
570 rBC deposition at the Dasuopu site is highest during the winter (non-monsoon) season
571 when westerly circulation is dominant. Back trajectory analyses indicate that this
572 westerly circulation predominantly includes areas of west/northwest India, Afghanistan,
573 Pakistan, northern Africa, central Europe and the Mediterranean. Dry conditions
574 increase the production of rBC through biomass burning and we suggest that regional
575 biomass burning contributes to periods of high rBC deposition onto the Dasuopu glacier
576 during periods of dryness as indicated by historical records of precipitation within the
577 atmospheric catchment of Dasuopu glacier. The continuous historical record of
578 precipitation for India, in particular, suggests an association between moderate to
579 severe drought conditions in west/north-west India and rBC concentration in the
580 Dasuopu ice core. Upwind industrial sources of rBC, such as coal combustion, appear
581 to be of minor influence during these periods of increased rBC deposition as indicated
582 by the absence of correlation between rBC concentration in the Dasuopu core and the
583 crustal enrichment of industrially-sourced trace elements at equivalent depths in the ice
584 core. It should be noted that the Dasuopu ice core rBC record is discontinuous during
585 the period of increased regional industrial activity thus the available data cannot
586 address the importance of this regional industrialization to rBC deposition onto Dasuopu



587 glacier. Together, evidence presented here indicates that while rBC transport in the free
588 troposphere is influenced by large scale synoptic circulation, regional sources of rBC
589 strongly influence rBC deposition onto Dasuopu glacier, particularly after ~1877, and
590 that the rBC record from Dasuopu glacier may provide a proxy record for drought and
591 resultant biomass burning within its catchment of atmospheric circulation.

592

593 **Acknowledgments**

594 This work was funded by the NSF Atmospheric Chemistry Program (award # 1149239)
595 and the by the NSF-ESH program, The Ohio State University, the Ohio State
596 Committee of Science and Technology, and the National Natural Science Foundation of
597 China. We thank the many scientists, engineers, technicians, and graduate students
598 from the Byrd Polar and Climate Research Center and the Lanzhou Institute of
599 Glaciology and Geocryology (China) that contributed to the collection and previous
600 analysis of the Dasuopu ice core. We are grateful to Julien Nicolas for performing the
601 graphic display of the back trajectories. This is BPCRC contribution no. xxxx.

602

603 **Data availability**

604 The data presented in this work are archived at the National Oceanic and Atmospheric
605 Administration World Data Center-A for Paleoclimatology at xxxx.

606

607 **Author contribution**

608 Barker performed the sample preparation, BC analysis and interpretation, and was the
609 primary author of the manuscript. Kaspari assisted with the BC analysis and
610 interpretation of the BC record. Gabrielli designed the overall project, performed the
611 trace element analysis with Wegner. Wegner, Beaudon, and Sierra-Hernández cut the
612 samples from the ice core and performed the trace element analysis. Thompson
613 retrieved the Dasuopu ice core. All authors contributed to manuscript preparation.

614

615 **Competing interests**

616 The authors declare that they have no conflict of interest.

617



618 References

- 619 Anchukaitis, K.J., Buckley, B.M., Cook, E.R., D'Arrigo, R.D., and Ammann, C.M.:
620 Influence of volcanic eruptions on the climate of the Asian monsoon region,
621 *Geophys. Res. Lett.*, 37, 1-5, doi: 10.1029/2010GL044843, 2010.
- 622 Babu, S.S., Chaubey, J.P., Moorthy, K.K., Gogoi, M.M., Kompalli, K.K., Sreekanth, V.,
623 Bagare, S.P., Bhatt, B.C., Gaur, V.K., Prabhu, T.P., and Singh, N.S.: High
624 altitude (~4520 m amsl) measurements of black carbon aerosols over western
625 trans-Himalayas: Seasonal heterogeneity and source apportionment, *J.*
626 *Geophys. Res.-Atmos.*, 116, D24201, doi: 10.1029/2011JD06722, 2011.
- 627 Baker, P.J., and Bunyavejchewin, S.: Fire behavior and fire effects across the forest
628 landscape of continental Southeast Asia. In: *Tropical Fire Ecology*. Springer
629 Praxis Books. Springer, Berlin, Heidelberg, doi: 10.1007/978-3-540-77381-8_11,
630 2009.
- 631 Bonasoni, P., Laj, P., Marinoni, A., Sprenger, M., Angelini, F., Arduini, J., Bonafe, U.,
632 Calzolari, F., Colombo, T., Decesari, S., Di Biagio, C., di Sarra, A.G., Evangelisti,
633 F., Duchi, R., Facchini, M.C., Fuzzi, S., Gobbi, G.P., Maione, M., Panday, A.,
634 Roccatò, F., Sellegri, K., Venzac, H., Verza, G.P., Villani, P., Vuillermoz, E., and
635 Cristofanelli, P.: Atmospheric brown clouds in the Himalayas: first two years of
636 continuous observations at the Nepal Climate Observatory-Pyramid (5079 m),
637 *Atmos. Chem. Phys.*, 10, 7515-7531, doi: 10.5194/acp-10-7515-2010, 2010.
- 638 Bond, T.C., Streets, D.G., Yarber, K.F., Nelson, S.M., Woo, J.-H., and Klimont, Z.: A
639 technology-based global inventory of black and organic carbon emissions from
640 combustion, *J. Geophys. Res. Atmos.*, 109, D14, doi: 10.1029/2003JD003697,
641 2004.
- 642 Bond, T.C., Bhardwaj, E., Dong, R., Jogani, R., Jung, S., Roden, C., Streets, D.G., and
643 Trautmann, N.M.: Historical emissions of black and organic carbon aerosol from
644 energy-related combustion, 1850-2000, *Global Biogeochem. Cy.*, 21, GB2018,
645 doi: 10.1029/2006GB002840, 2007.
- 646 Bond, T.C., Doherty, S.J., Fahey, D.W., Forster, P.M., Bernsten, T., DeAngelo, B.J.,
647 Flanner, M.G., Ghan, S., Karcher, B., Koch, D., Kinne, S., Kondo, Y., Quinn,
648 P.K., Sarofim, M.C., Schultz, M.G., Shulz, M., Venkataraman, C., Zhang, H.,
649 Zhang, S., Bellouin, N., Guttikunda, S.K., Hopke, P.K., Jaconson, M.Z., Kaiser,
650 J.W., Klimont, Z., Lohmann, U., Schwarz, J.P., Shindell, D., Storelvmo, T.,
651 Warren, S.G. and Zender, C.S.: Bounding the role of black carbon in the climate
652 system: A scientific assessment, *J. Geophys. Res.-Atmos.*, 118, 5380-5552, doi:
653 10.1002/jgrd.50171, 2013.
- 654 Cao, J., Tie, X., Xu, B., Zhao, Z., Zhu, C., Li, G., and Liu, S.: Measuring and modeling
655 black carbon (BC) contamination in the SE Tibetan Plateau, *J. Atmos. Chem.*,
656 67, 45-60, doi: 10.1007/s10874-011-9202-5, 2010.
- 657 Chaubey, J.P., Babu, S.S., Gogoi, M.M., Kompalli, S.K., Sreekanth, V., Moorthy, K.K.,
658 and Prabhu, T.P.: Black carbon aerosol over a high altitude (~ 4.52 km) station in
659 Western Indian Himalayas, *J. Inst. Eng.*, 8, 42-51, doi: 10.3126/jie.v8i3.5930,
660 2011.
- 661 Chen, X., Kang, S., Cong, Z., Yang, J., and Ma, Y.: Concentration, temporal variation



- 662 and sources of black carbon in the Mount Everest region retrieved by real-time
663 observation and simulation, *Atmos. Chem. Phys.*, 18, 12859-12875, doi:
664 10.5194/acp-18-12859-2018, 2018.
- 665 Cole-Dai, J., Ferris, D., Lanciki, A., Savarino, J., Baroni, M., and Thiemens, M.H.: Cold
666 decade (AD 1810-1819) caused by Tambora (1815) and another (1809)
667 stratospheric volcanic eruption, *Geophys. Res. Lett.*, 36, L22703, doi:
668 10.1029/2009GL040882, 2009
- 669 Cook, E.R., Anchukaitis, K.J., Buckley, B.M., D'Arrigo, R.D., Jacoby, G.C., and Wright,
670 W.E.: Asian monsoon failure and megadrought during the last millennium,
671 *Science*, 328, 486-489, doi: 10.1126/science.1185188, 2010.
- 672 Cook, E.R., Seager, R., Kushnir, Y., Briffa, K.R., Buntgen, U., Frank, D., Krusic, P.J.,
673 Tegel, W., van der Schrier, G., Andreu-Hayles, L., Baillie, M., Baittinger, C.,
674 Bleicher, N., Bonde, N., Brown, D., Carrer, M., Cooper, R., Cufar, K., Dittmar, C.,
675 Esper, J., Griggs, C., Gunnarson, B., Gunther, B., Gutierrez, E., Haneca, K.,
676 Helama, S., Herzig, F., Heussner, K.-U., Hofmann, J., Janda, P., Kontic, R.,
677 Kose, N., Kynცი, T., Levanic, T., Linderholm, H., Manning, S., Melvin, T.M., Miles,
678 D., Neuwirth, B., Nicolussi, K., Nola, P., Panayotov, M., Popa, I., Rothe, A.,
679 Seftigen, K., Seim, A., Svarva, H., Svoboda, M., Thun, T., Timonen, M.,
680 Touchan, R., Trotsiuk, V., Trouet, V., Walder, F., Wazny, T., Wilson, R., and
681 Zang, C.: Old world megadroughts and pluvials during the Common Era, *Sci.*
682 *Adv.*, 1, doi: 10.1126/sciadv.1500561, 2015
- 683 Davis, M.E., Thompson, L.G., Yao, T., and Wang, N.: Forcing of the Asian monsoon on
684 the Tibetan Plateau: Evidence from high-resolution ice core and tropical coral
685 records, *J. Geophys. Res.*, 110, D04101, doi: 10.1029/2004JD004933, 2005.
- 686 Debret, M., Bout-Roumazielles, V., Grousset, F., Desmet, M., McManus, J.F., Massei,
687 N., Sebag, D., Petit, J.-R., Copard, Y., and Trentesaux, A.: The origin of the
688 1500-year climate cycles in Holocene North-Atlantic records, *Clim. Past Discuss.*,
689 3, 679-692, doi: 10.5194/cp-3-569-2007, 2007.
- 690 Debret, M., Sebag, D., Costra, X., Massei, N., Petit, J.-R., Chapron, E., and Bout-
691 Roumazielles, V.: Evidence from wavelet analysis for a mid-Holocene transition
692 in global climate forcing, *Quaternary Sci. Rev.*, 28, 2675-2688, doi:
693 10.1016/j.quascirev.2009.06.005, 2009.
- 694 Doherty, S.J., Grenfell, T.C., Forsström, Hagg, D.L., Brandt, R.E., and Warren, S.G.:
695 Observed vertical redistribution of black carbon and other insoluble light-
696 absorbing particles in melting snow, *J. Geophys. Res. Atmos.*, 118, 5553-5569,
697 doi: 10.1002/jgrd.50235, 2013.
- 698 Echalar, F., Gaudichet, A., Cachier, H., and Artaxo, P.: Aerosol emissions by tropical
699 forest and savanna biomass burning: characteristic trace elements and fluxes,
700 *Geophys. Res. Lett.*, 22, 3039-3042, doi: 10.1029/95GL03170, 1995.
- 701 Flanner, M. G., Zender, C. S., Randerson, J. T., and Rasch, P. J.: Present day climate
702 forcing and response from black carbon in snow, *J. Geophys. Res.*, 112,
703 D11202, doi:10.1029/2006JD008003, 2007.
- 704 Forster, P., Ramaswamy, V., Artaxo, P., Berntsen, T., Betts, R., Fahey, D.W., Haywood,
705 J., Lean, J., Lowe, D.C., Myhre, G., Nganga, J., Prinn, R., Raga, G., Schulz, M.,
706 and Van Dorland, R. Miller, H.L. (Ed.). (2007). *Changes in Atmospheric*



- 707 Constituents and in Radiative Forcing Chapter 2. United Kingdom: Cambridge
708 University Press.
- 709 Gabrielli, P., Wegner, A., Sierra Hernández, R., Beaudon, E., Davis, M., Barker, J.D.,
710 and Thompson, L.G., Early contamination of the Himalayan atmosphere from
711 coal combustion since the onset of the European Industrial Revolution (~1780
712 A.D.), *P. Natl. Acad. Sci. USA*, doi: 10.1073/pnas.1910485117, 2020.
- 713 Gaudichet, A., Echalar, F., Chatenet, B., Quisefit, J.P., and Malingre, G.: Trace
714 elements in tropical African savanna biomass burning aerosols, *J. Atmos. Chem.*,
715 22, 19-39, doi: 10.1007/BF00708179, 1995.
- 716 Gertler, C.G., Puppala, S.P., Panday, A., Stumm, D., and Shea, J.: Black carbon and
717 the Himalayan cryosphere: A review, *Atmos. Env.*, 125, 404-417, doi:
718 10.1016/j.atmosenv.2015.08.078, 2016.
- 719 Gilardoni, S., and Fuzzi, S.: Chemical composition of aerosols of different origin. *in*
720 Tomasi, C., Fuzzi, S., and Kokhanovsky, A. (eds): *Atmospheric Aerosols: Life*
721 *Cycles and Effects of Air Quality and Climate*. Wiley-VCH Verlag GmbH & Co.
722 KGaA, Weinheim, 183-221, doi: 10.1002/9783527336449.ch4, 2017.
- 723 Ginot, P., Dumont, M., Lim, S., Patris, N., Taupin, J.-D., Wagnon, P., Gilbert, A.,
724 Arnaud, Y., Marinoni, A., Bonasoni, P., and Laj, P.: A 10 year record of black
725 carbon and dust from a Mera Peak ice core (Nepal): variability and potential
726 impact on melting of Himalayan glaciers, *Cryosphere*, 8, 1479-1496, doi:
727 10.5194/tc-8-1479-2014, 2014.
- 728 Hammes, K., Schmidt, M. W. I., Smernik, R. J., Currie, L. A., Ball, W. P., Nguyen, T. H.,
729 Louchouart, P., Houel, S., Gustafsson, Ö., Elmquist, M., Cornelissen, G.,
730 Skjemstad, J. O., Masiello, C. A., Song, J., Peng, P., Mitra, S., Dunn, J. C.,
731 Hatcher, P. G., Hockaday, W. C., Smith, D. M., Hartkopf-Fröder, C., Böhmer, A.,
732 Lüer, B., Huebert, B. J., Amelung, W., Brodowski, S., Huang, L., Zhang, W.,
733 Gschwend, P. M., Flores-Cervantes, D. X., Largeau, C., Rouzaud, J., Rumpel,
734 C., Guggenberger, G., Kaiser, K., Rodionov, A., Gonzalez-Vila, F. J., Gonzalez-
735 Perez, J. A., de la Rosa, J. M., Manning, D. A. C., López-Capél, E., and Ding, L.,
736 Comparison of quantification methods to measure fire-derived (black/elemental)
737 carbon in soils and sediments using reference materials from soil, water,
738 sediment and the atmosphere, *Global Biogeochem. Cy.*, 21, GB3016,
739 doi:10.1029/2006GB002914, 2007.
- 740 Hansen, J., and Nazarenko, L.: Soot climate forcing via snow and ice albedos, *P. Natl.*
741 *Acad. Sci. USA*, 101, 423-428, doi: 10.1073/pnas.2237157100, 2004.
- 742 Hill, A.F., Rittger, K., Dendup, T., Tshering, D. and Painter, T.H.: How important is
743 meltwater to the Chamkhar Chhu headwaters of the Brahmaputra River?, *Front.*
744 *Earth. Sci.*, 8, 81, doi: 10.3389/feart.2020.00081, 2020.
- 745 Immerzeel, W.W., van Beek, L.P.H., and Bioerkens, M.F.P.: Climate change will affect
746 the Asian water towers, *Science*, 328, 1382-1385, doi: 10.1126/science.1183188,
747 2010.
- 748 IPCC: *Climate Change 2013: The Physical Science Basis. Contribution of*
749 *Working Group I to the Fifth Assessment Report of the Intergovernmental Panel*
750 *on Climate Change*. Stocker, T.F., D. Qin, G.-K. Plattner, M. Tignor, S.K. Allen, J.
751 Boschung, A. Nauels, Y. Xia, V. Bex and P.M. Midgley (Ed.). Cambridge



- 752 University Press, Cambridge, United Kingdom and New York, NY, USA, 1535 pp,
753 doi:10.1017/CBO9781107415324, 2013.
- 754 Jacobson, M. Z.: Climate response of fossil fuel and biofuel soot, accounting for soot's
755 feedback to snow and sea ice albedo and emissivity, *J. Geophys. Res.*, 109,
756 D21201, doi:10.1029/2004JD004945, 2004.
- 757 Jenkins, M., Kaspari, S., Kang, S.-C., Grigholm, B., and Mayewski, P.A.: Tibetan
758 Plateau Geladaindong black carbon ice core record (1843-1982): Recent
759 increases due to higher emissions and lower snow accumulation, *Adv. Clim.
760 Change Res.*, 7, 132-138, doi: 10.1016/j.accre.2016.07.002, 2016.
- 761 Kaspari, S., Painter, T.H., Gysel, M., Skiles, S.M., and Schwikowski, M.: Seasonal and
762 elevational variations of black carbon and dust in snow and ice in the Solu-
763 Khumbu, Nepal and estimated radiative forcings, *Atmos. Chem. Phys.*, 14, 8089-
764 8103, doi: 10.5194/acp-14-8089-2014, 2014.
- 765 Kaspari, S.D., Schwikowski, M., Gysel, M., Flanner, M.G., Kang, S., Hou, S., and
766 Mayewski, P.A.: Recent increase in black carbon concentrations from a Mt.
767 Everest ice core spanning 1860-2000 AD, *Geophys. Res. Lett.*, 38, L04703, doi:
768 10.1029/2010GL046096, 2011.
- 769 Kopacz, M., Mauzerall, D.L., Wang, J., Leibensperger, E.M., Henze, D.K., and Singh,
770 K.: Origin and radiative forcing of black carbon transported to the Himalayas and
771 Tibetan Plateau, *Atmos. Chem. Phys.*, 11, 2837-2852, doi: 10.5194/acp-11-2837-
772 2011, 2011.
- 773 Kumar, R., Barth, M.C., Pfister, G.G., Nair, V.S., Ghude, S.D., and Ojha, N.: What
774 controls the seasonal cycle of black carbon aerosols in India?, *J. Geophys. Res.
775 Atmos.*, 120, 7788-7812, doi: 10.1002/2015JD023298, 2015.
- 776 Lack, D.A., Moosmüller, H., McMeeking, G.R., Chakrabarty, R.K., and Baumgardner,
777 D.: Characterizing elemental, equivalent black, and refractory black carbon
778 aerosol particles: a review of techniques, their limitations and uncertainties, *Annl.
779 Bioanal. Chem.*, 406, 99-122, doi: 10.1007/s00216-013-7402-3, 2014.
- 780 Lau, W.K.M., and Kim, K.M.: Fingerprinting the impacts of aerosols on long-term trends
781 of the Indian summer monsoon regional rainfall, *Geophys. Res. Lett.*, 37,
782 L16705, doi: 10.1029/2010GL043255, 2010.
- 783 Lee, Y.H., Lamarque, J.-F., Flanner, M.G., Jiao, C., Shindell, D.T., Bernsten, T.,
784 Bisiaux, M.M., Cao, J., Collins, W.J., Curran, M., Edwards, R., Faluvegi, G.,
785 Ghan, S., Horowitz, L.W., McConnell, J.R., Ming, J., Myhre, G., Nagashima, T.,
786 Naik, V., Rumbold, S.T., Skeie, R.B., Sudo, K., Takemura, T., Thevenon, F., Xu,
787 B., and Yoon, J.-H.: Evaluation of preindustrial to present-day black carbon and
788 its albedo forcing from Atmospheric Chemistry and Climate Model
789 Intercomparison Project (ACCMIP), *Atmos. Chem. Phys.*, 13, 2607-2634,
790 doi:10.5194/acp-13-2607-2013, 2013.
- 791 Lelieveld, J., Bourtsoukidis, E., Bruhl, C., Fischer, H., Fuchs, H., Harder, H.,
792 Hofzumahaus, A., Holland, F., Marno, D., Neumaier, M., Pozzer, A., Schlager,
793 H., Williams, J., Zahn, A., and Ziereis, H.: The South Asian monsoon – pollution
794 pump and purifier, *Science*, 361, 270-273, doi: 10.1126/science.aar2501, 2018.
- 795 Li, S., Yao, T., Tian, L., and Wang, P.: Seasonal transition characteristics of the



- 796 westerly jet: Study based on field observations at an altitude of 6900 m on the
797 Mt. Xixiabangma Dasuopu glacier, Chinese Sci. Bull., 56, 1912-1920, doi:
798 10.1007/s11434-011-4508-x, 2011.
- 799 Lindberg, J.D., Douglass, R.E., and Garvey, D.M.: Atmospheric particulate absorption
800 and black carbon measurement, *Appl. Optics*, 38, 2369-2376, doi:
801 10.1364/AO.38.002369, 1999.
- 802 Liu, X., Xu, B., Yao, T., Wang, N., and Wu, G.: Carbonaceous particles in Muztagh Ata
803 ice core, west Kunlun mountains, China, *Chin. Sci. Bull.*, 53, doi:
804 10.1007/s11434-008-0294-5, 2008.
- 805 Lund, M.T., Samset, B.H., Skeie, R.B., Watson-Parris, D., Katich, J.M., Schwarz, J.P.,
806 and Weinzierl, B.: Short black carbon lifetime inferred from a global set of aircraft
807 observations, *NPJ Climate and Atmospheric Science*, 1, doi: 10.1038/s41612-
808 018-0040-x, 2018.
- 809 Marinoni, A., Cristofanelli, P., Laj, P., Duchi, R., Calzolari, F., Decesari, S., Sellegri, K.,
810 Vuillermoz, E., Verza, G.P., Villani, P., and Bonasoni, P.: Aerosol mass and black
811 carbon concentrations, a two year record at NCO-P (5079 m, Southern
812 Himalayas), *Atmos. Chem. Phys.*, 10, 8551-8562, doi: 10.5194/acp-10-8551-
813 2010, 2010.
- 814 Marinoni, A., Cristofanelli, P., Laj, P., Duchi, R., Putero, D, Calzolari, F., Landi, T.C.,
815 Vuillermoz, E., Maione, M., and Bonasoni, P.: High black carbon and ozone
816 concentrations during pollution transport in the Himalayas: five years of
817 continuous observations at NCO-P global GAW station, *J. Environ. Sci. (China)*,
818 25, 1618-1625, doi: 10.1016/S1001-0742(12)60242-3, 2013.
- 819 Ming, J., Cachier, H., Xiao, C., Qin, D., Kang, S., Hou, S, and Xu, J.: Black carbon
820 record based on a shallow Himalayan ice core and its climatic implications.
821 *Atmos. Chem. Phys.*, 8, 1343–52, doi: 10.5194/acp-8-1343-2008, 2008.
- 822 Ming, J., Du, Z., Xiao, C., Xu, X., and Zhang, D.: Darkening of the mid-Himalaya
823 glaciers since 2000 and the potential causes, *Environ. Res. Lett.*, 7, 014021, doi:
824 10.1088/1748-9326/7/1/014021, 2012.
- 825 Mishra, V., Tiwari, A.D., Aadhar, S., Shah, R., Xiao, M., Pai, D.S., and Lettenmaier, D.:
826 Drought and famine in India, 1870-2016, *Geophys. Res. Lett.*, 46, 2075-2083,
827 doi: 10.1029/2018GL081477, 2019.
- 828 Montanari, L., Basu, B., Spagnoli, A., and Broderick, B.M.: A padding method to reduce
829 edge effects for enhanced damage identification using wavelet analysis, *Mech.*
830 *Syst. Signal Pr.*, 52-52, 264-277, doi: 10.1016/j.ymsp.2014.06.014, 2015.
- 831 Mooley, D.A., Parthasarathy, B., Sontakke, N.A., Munot, A.A.: Annual rain-water over
832 India, its variability and impact on the economy, *J. Climatol.*, 1, 167-186, doi:
833 10.1002/joc.3370010206, 1981.
- 834 Nair, V.S., Babu, S.S., Moorthy, K.K., Sharma, A.K., Marinoni, A., and Ayai: Black
835 carbon aerosols over the Himalayas: direct and surface albedo forcing, *Tellus*
836 *Ser. B Chem. Phys. Meteorol.*, 65, 1-14, doi: 10.3402/tellusb.v65i0.19738, 2013.
- 837 Negi, P.S., Pandey, C.P., and Singh, N.: Black carbon aerosol in the ambient air of
838 Gangotri Glacier valley of north-western Himalaya in India, *Atmos. Environ.*, 214,
839 116879, doi: 10.1016/j.atmosenv.2019.116879, 2019.
- 840 Niu, H., Kang, S., Shi, X., Paudyal, R., He, Y., Li, G., Wang, S., Pu, T., and Shi, X.: In-



- 841 situ measurements of light-absorbing impurities in snow of glacier on Mt. Yulong
842 and implications for radiative forcing estimates, *Sci. Total Environ.*, 581-582, 848-
843 856, doi: 10.1016/j.scitotenv.2017.01.032, 2017.
- 844 Novakov, T., Ramanathan, V., Hansen, J.E., Kirchstetter, T.W., Sato, M., Sinton, J.E.,
845 and Sathaye, J.A., Large historical changes of fossil-fuel black carbon aerosols,
846 *Geophys. Res. Lett.*, 30, 1324, doi: 10.1029/2002GL016345, 2003.
- 847 Ogren, J.A., and Charlson, R.J.: Elemental carbon in the atmosphere: cycle and
848 lifetime, *Tellus*, 35B, 241-254, doi: 10.1111/j.1600-0889.1983.tb00027.x, 1983.
- 849 Parthasarathy, B., Sontakke, N.A., Monot, A.A., and Kothawale, D.R.: Droughts/floods
850 in the summer monsoon season over different meteorological subdivisions of
851 India for the period 1871-1984, *Int. J. Climatol.*, 7, 57-70, doi:
852 10.1002/joc.3370070106, 1987.
- 853 Rahaman, W., Chatterjee, S., Ejaz, T., and Thamban, M.: Increased influence of ENSO
854 on Antarctic temperature since the Industrial Era, *Sci. Rep-UK.*, 9, 6006, doi:
855 10.1038/s41598-019-42499-x, 2019.
- 856 Ramanathan, V. and Carmichael, G.: Global and regional climate changes due to black
857 carbon, *Nature Geosci.*, 1, 221–227, doi:10.1038/ngeo156, 2008.
- 858 Ramanathan, V., Ramana, M.V., Roberts, G., Kim, D., Corrigan, C., Chung, C., and
859 Winker, D.: Warming trends in Asia amplified by brown cloud solar absorption,
860 *Nature*, 448, 575-578, doi: 10.1038/nature06019, 2007.
- 861 Reddy, M.S., and Boucher, O.: A study of the global cycle of carbonaceous aerosols in
862 the LMDZT general circulation model, *J. Geophys. Res.*, 109, D14202, doi:
863 10.1029/2003JD0040-48, 2004.
- 864 Reddy, M.S., and Boucher, O.: Climate impact of black carbon emitted from energy
865 consumption in the world's regions, *Geophys. Res. Lett.*, 34, L11802, doi:
866 10.1029/2006GL028904, 2007.
- 867 Ross, A.B., Jones, J.M., Chaiklangmuang, S., Pourkashanian, M., Williams, A., Kubica,
868 K., Andersson, J.T., Kerst, M., Danihelka, P., and Bartle, K.D.: Measurement and
869 prediction of the emission of pollutants from the combustion of coa and biomass
870 in a fixed bed furnace, *Fuel*, 81, 571-582, doi:10.1016/S0016-2361(01)00157-0,
871 2002.
- 872 Sakai, A., and Fujita, K.: Contrasting glacier response to recent climate change in
873 high-mountain Asia, *Sci. Rep-UK*, 7, 13717, doi: 10.1038/s41598-017-
874 14256-5, 2017.
- 875 Samset, B.H., Myhre, G., Herber, A., Kondo, Y., Li, S.-M., Moteki, N., Koike, M.,
876 Oshima, N., Schwarz, J.P., Balkanski, Y., Bauer, S.E., Bellouin, N., Berntsen,
877 T.K., Bian, H., Chin, M., Diehl, T., Easter, R.C., Ghan, S.J., Iversen, T., Kirkevag,
878 A., Lamarque, J.-F., Lin, G., Liu, X., Penner, J.E., Schulz, M., Seland, O., Skeie,
879 R.B., Stier, P., Takemura, T., Tsigardis, K., and Zhang, K.: Modelled black
880 carbon radiative forcing and atmospheric lifetime in AeroCom Phase II
881 constrained by aircraft observations, *Atmos. Chem., Phys.*, 14, 12465-12477,
882 doi: 10.5194/acp-14-12465-2014, 2014.
- 883 Samsonov, Y.N., Ivanov, V.A., McRae, D.J., and Baker, S.P.: Chemical and dispersal
884 characteristics of particulate emissions from forest fires in Siberia, *Int. J. Wildland
885 Fire*, 21, 818-827, doi: 10.1071/WF11038, 2012.
- 886 Schwarz, J.P., Gao, R.S., Fahey, D.W., Thomson, D.S., Watts, L.A., Wilson, J.C.,



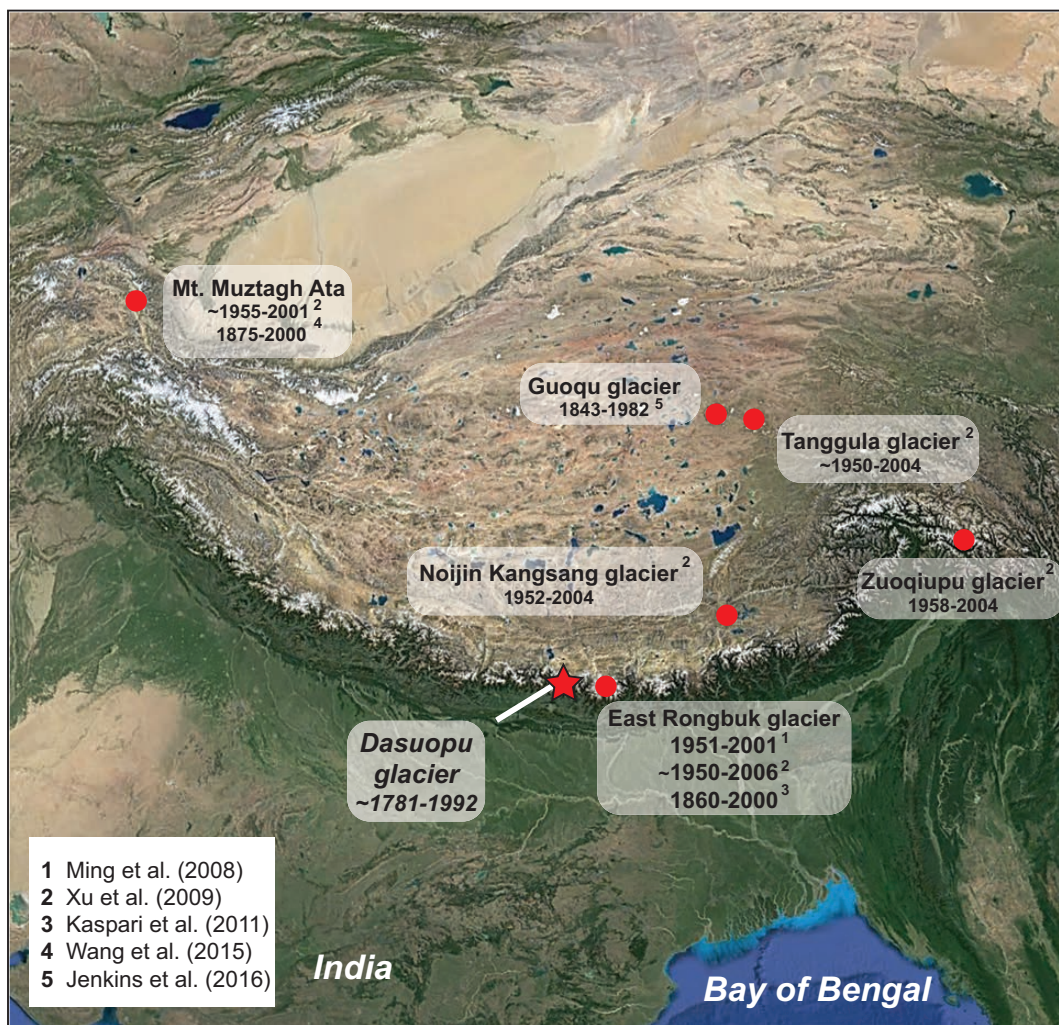
- 887 Reeves, J.M., Darbeheshti, M., Baumgardner, D.G., Kok, G.L., Chung, S.H.,
888 Schulz, M., Hendricks, J., Lauer, A., Karcher, B., Slowik, J.G., Rosenlof, K.H.,
889 Thompson, T.L., Langford, A.O., Loewenstein, M., and Aikin, K.C.: Single-particle
890 measurements of midlatitude black carbon and light-scattering aerosols from the
891 boundary layer to the lower stratosphere, *J. Geophys. Res. Atmos.*, 111,
892 D16207, doi: 10.1029/2006JD007076, 2006.
- 893 Scott, C.A., Zhang, F., Mukherji, A., Immerzeel, W., Mustafa, D., and Bharati, L.: Water
894 in the Hindu Kush Himalaya. In: Wester, P., Mishra, A., and Shrestha, A. (eds):
895 The Hindu Kush Himalaya Assessment. Springer, Cham, doi: 10/1007/978-3-
896 319-92288-1_8, 2019.
- 897 Stothers, R.B.: The great Tambora eruption in 1815 and its aftermath, *Science*, 224,
898 1191-1198, doi: 10.1126/science.224.4654.1191, 1984.
- 899 Su, H., Liu, Q., and Li, J.: Alleviating border effects in wavelet transforms for nonlinear
900 time-varying signal analysis, *Adv. Electr. Comput. En.*, 11, 55-60, doi:
901 10.4316/AECE.2011.03009, 2011.
- 902 Thapa, U.K., St. George, S., Kharal, D.K., and Gaire, N.P.: Tree growth across the
903 Nepal Himalaya during the last four centuries, *Prog. Phys. Geog.*, 41, 478-495,
904 doi: 10.1177/0309133317714247, 2017.
- 905 Thind, P.S., Chandel, K.K., Sharma, S.K., Mandal, T.K., and John, S.: Light-absorbing
906 impurities in snow of the Indian Western Himalayas: impact on snow albedo,
907 radiative forcing, and enhanced melting, *Environ. Sci. Pollut. R.*, 26, 7566-7578,
908 doi: 10.1007/S11356-019-04183-5, 2019.
- 909 Thompson, L.G., Yao, T., Mosley-Thompson, E., Davis, M.E., Henderson, K.A., and Lin,
910 P.-N.: A high-resolution millennial record of the south Asian monsoon from
911 Himalayan ice cores, *Science*, 289, 1916-1919, doi:
912 10.1126/science.289.5486.1916, 2000.
- 913 Torrence, C., and Compo, G.P.: A practical guide to wavelet analysis, *B. Am. Meteorol.*
914 *Soc.*, 79, 61-78, doi: 10.1175/1520-0477(1998)079<0061:APGTWA>2.0.CO;2,
915 1998.
- 916 Tosca, M.G., Randerson, J.T., Zender, C.S., Flanner, M.G., and Rasch, P.J.: Do
917 biomass burning aerosols intensify drought in equatorial Asia during El Niño?,
918 *Atmos. Chem. Phys.*, 10, 3515-3528, doi: 10.5194/acpd-9-23319-2009, 2010.
- 919 Uglietti, C., Gabrielli, P., Olesik, J.W., Lutton, A., and Thompson, L.G.: Large variability
920 of trace element mass fractions determined by ICP-SFMS in ice core samples
921 from worldwide high altitude glaciers, *Appl. Geochem.*, 47, 109-121, doi:
922 10.1016/j.apgeochem.2014.05.019, 2014.
- 923 Wang, M., Xu, B., Kaspari, S.D., Gleixner, G., Schwab, V.F., Zhao, H., Wang, H., and
924 Yao, P.: Century-long record of black carbon in an ice core from the Eastern
925 Pamirs: Estimated contributions from biomass burning, *Atmos. Env.*, 115, 79-88,
926 doi: 10.1016/j.atmosenv.2015.05.034, 2015.
- 927 Wendl, I.A., Menking, J.A., Färber, R., Gysel, M., Kaspari, S.D., Laborde, M.J.G., and
928 Schwikowski, M.: Optimized method for black carbon analysis in ice and snow
929 using the Single Particle Soot Photometer, *Atmos. Meas. Tech.*, 7, 2667-2681,
930 doi: 10.5194/amt-7-2667-2014, 2014.
- 931 Xu, B., Cao, J., Hansen, J., Yao, T., Joswia, D.R., Wang, N., Wu, G., Wang, M., Zhao,



- 932 H., Yang, W., Liu, X., and He, J.: Black soot and the survival of Tibetan glaciers,
933 P. Natl. Acad. Sci. USA, 106, 22114-22118, doi: 10.1073/pnas.0910444106,
934 2009.
- 935 Yang, M., Yao, T., Wang, H., and Gou, X.: Climatic oscillations over the past 120 kyr
936 recorded in the Guliya ice core, China, Quatern. Int., 154-155, 11-18, doi:
937 10.1016/j.quaint.2006.02.015, 2006.
- 938 Zhang, Y., Kang, S., Sprenger, M., Cong, Z., Gao, T., Li, C., Tao, S., Li, X., Zhong, X.,
939 Xu, M., Meng, W., Neupane, B., Qin, X., and Sillanpaa, M.: Black carbon and
940 mineral dust in snow cover on the Tibetan Plateau, The Cryosphere, 12, 413-
941 431, doi: 10.5194/tc-12-413-2018, 2018.
- 942



943 Figure 1:



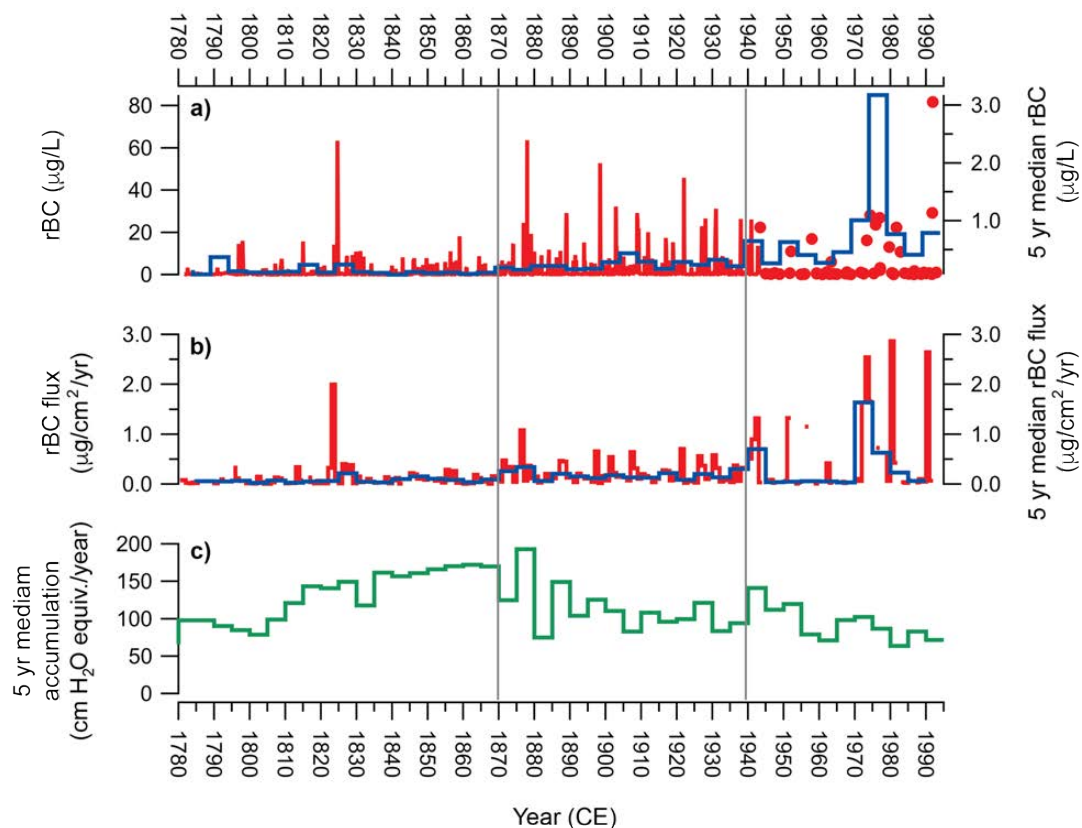
Source: "Tibetan Plateau" 28.38°N, 85.72°E. © Google Earth, Image: Landsat / Copernicus. 11/30/2016. 11/20/2019.

944

945 Fig. 1: The location of Dasuopu glacier, Mt. Xixiabangma and the location of other ice
946 cores that have provided a historical record of BC deposition in the region. The span of
947 each BC record is indicated.
948



949 Figure 2:

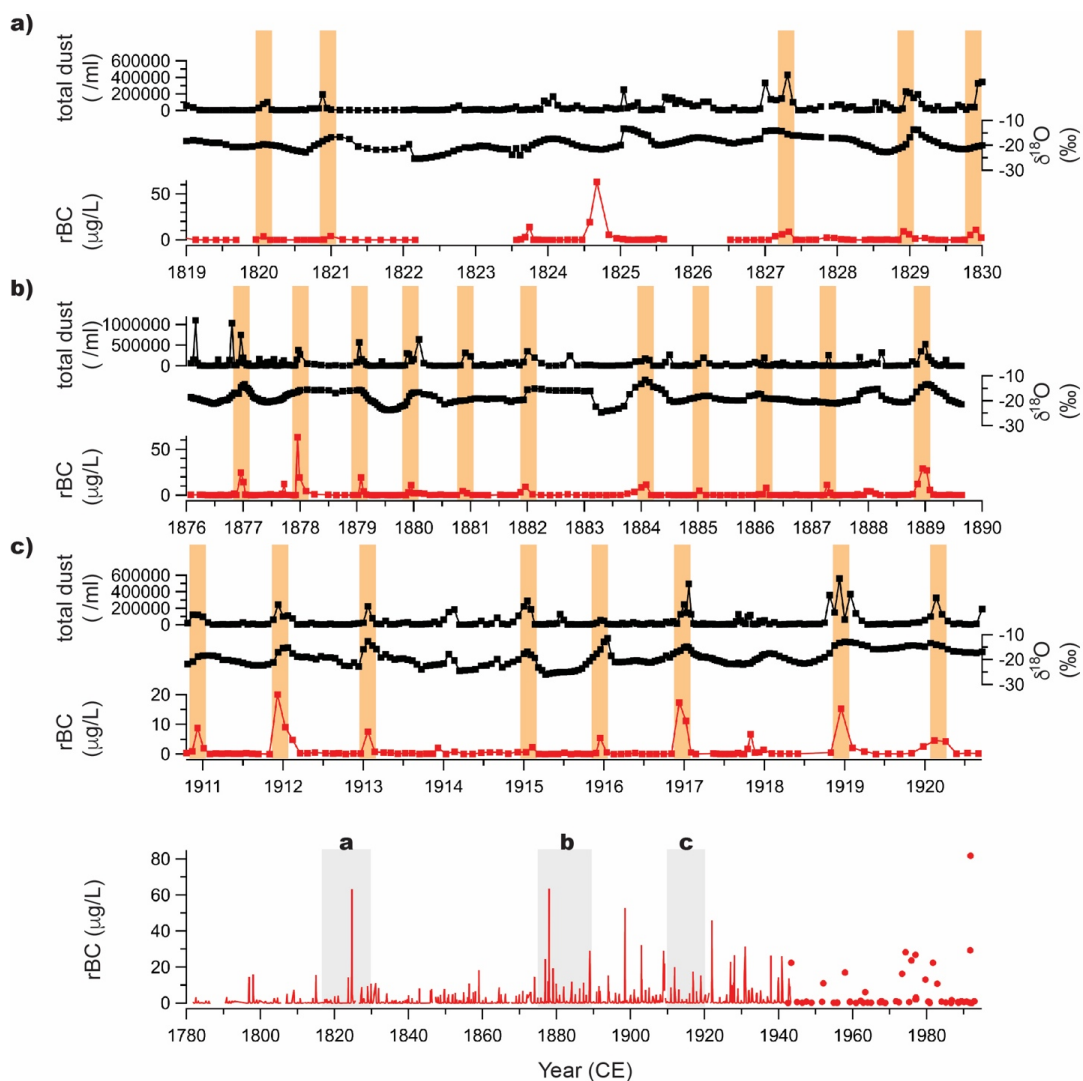


950

951 Fig. 2: a) the rBC record from the Dasuopu ice core (red). Red dots indicate discrete firn
952 samples. The 5 year median is indicated (blue); b) the rBC deposition flux onto
953 Dasuopu glacier (red) with the 5 year median (blue); c) the annual snow accumulation
954 record for the Dasuopu ice core (Davis et al., 2005).
955



956 Figure 3:

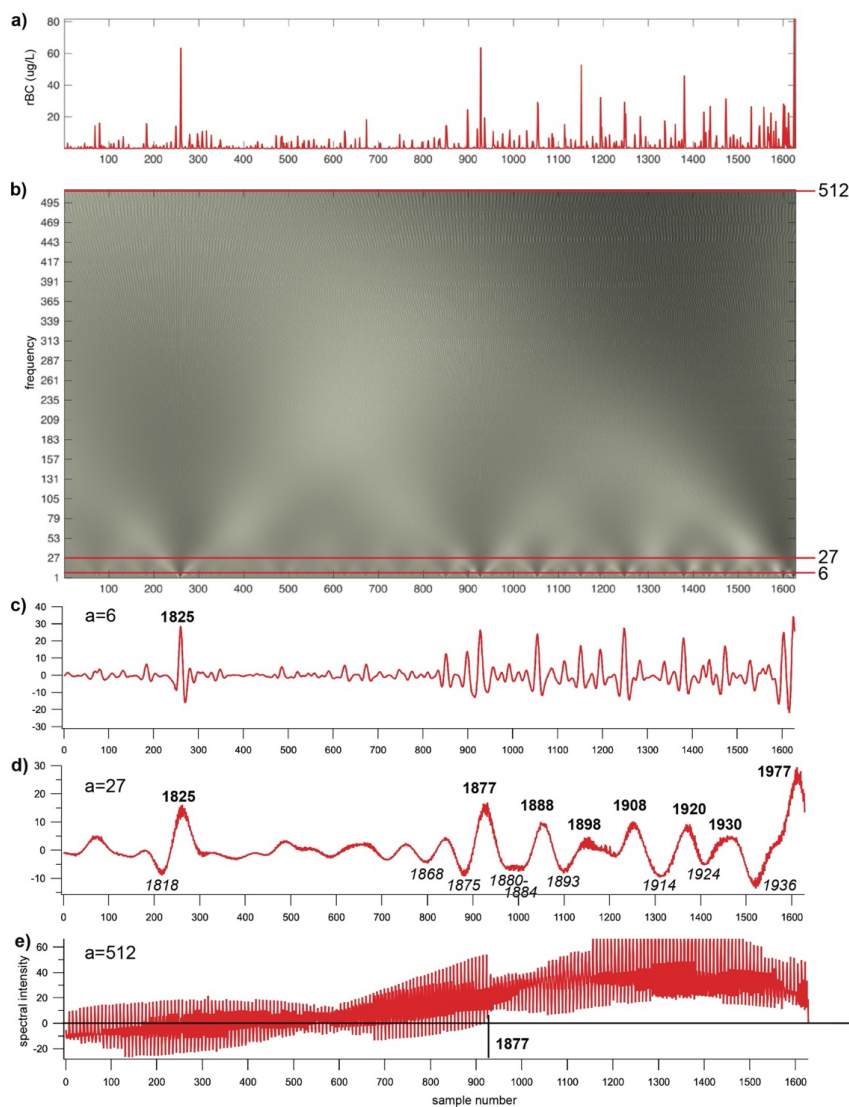


957
958
959
960
961
962

Fig. 3: Peaks in the rBC record compared to the total dust and $\delta^{18}\text{O}$ records (Thompson et al., 2000) over 3 time intervals (a: 1819 - 1830, b: 1876 - 1890, c: 1911 - 1921 CE) in the Dasuopu ice core. Note that peaks in the rBC record are associated with depleted $\delta^{18}\text{O}$ and increased dust deposition.



963 Figure 4:

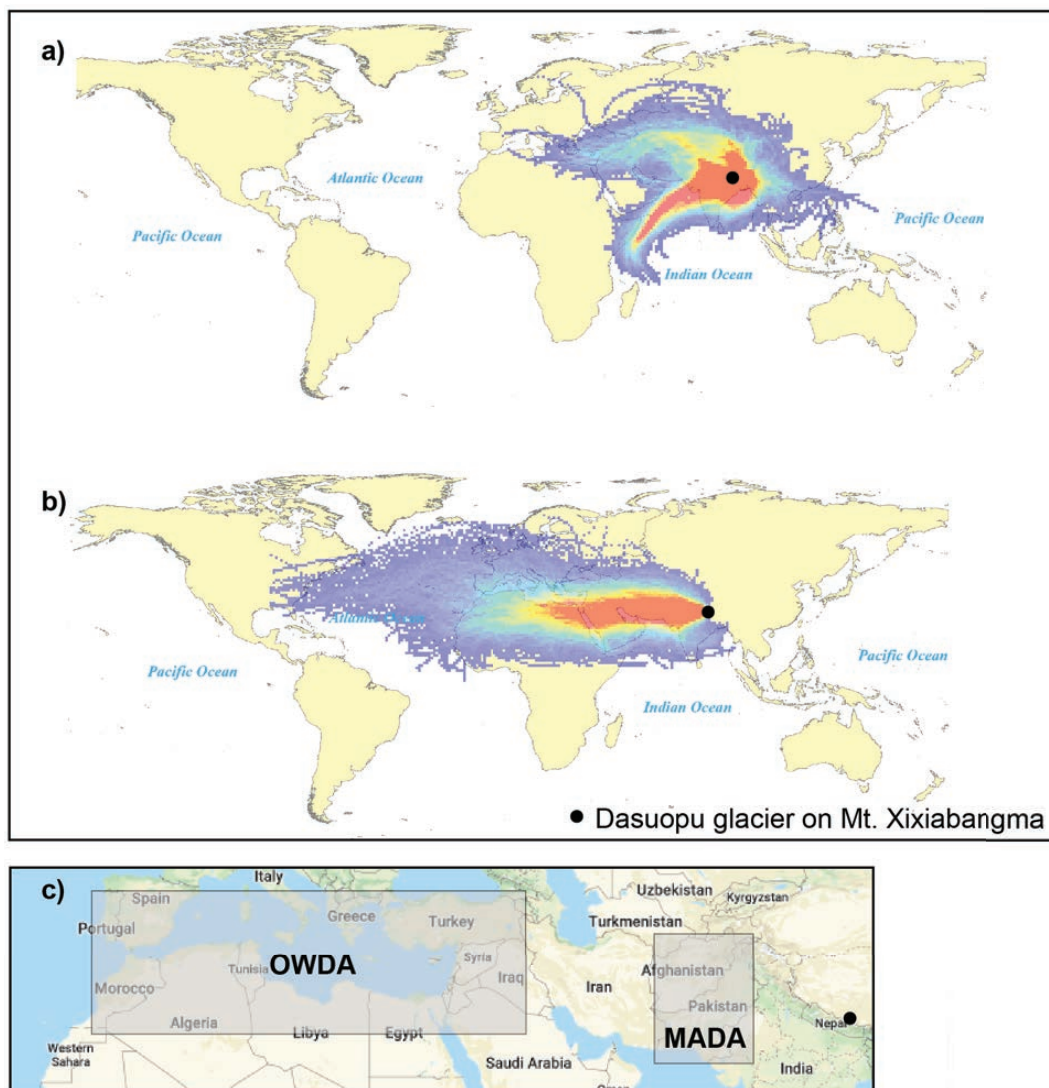


964

965 Fig. 4: The spectral analysis of the Dasuopu rBC concentration record. Sample number
966 1 is located at the bottom of the ice core (1781 CE) and sample number 1628 is at the
967 top of the firn section (1992 CE). a) is the rBC record plotted relative to sample number;
968 b) is the spectral analysis showing variance across all frequency scales relative to
969 sample number ranging from $a = 2$ to $a = 512$. Darker shades indicate relatively
970 stronger (more positive) coherence between the wavelet and the rBC record, as
971 indicated in the spectral coefficients; c, d, e) are the spectral coefficients relative to
972 sample number for frequency scales $a = 6$, 27 , and 512 respectively.
973



974 Figure 5:



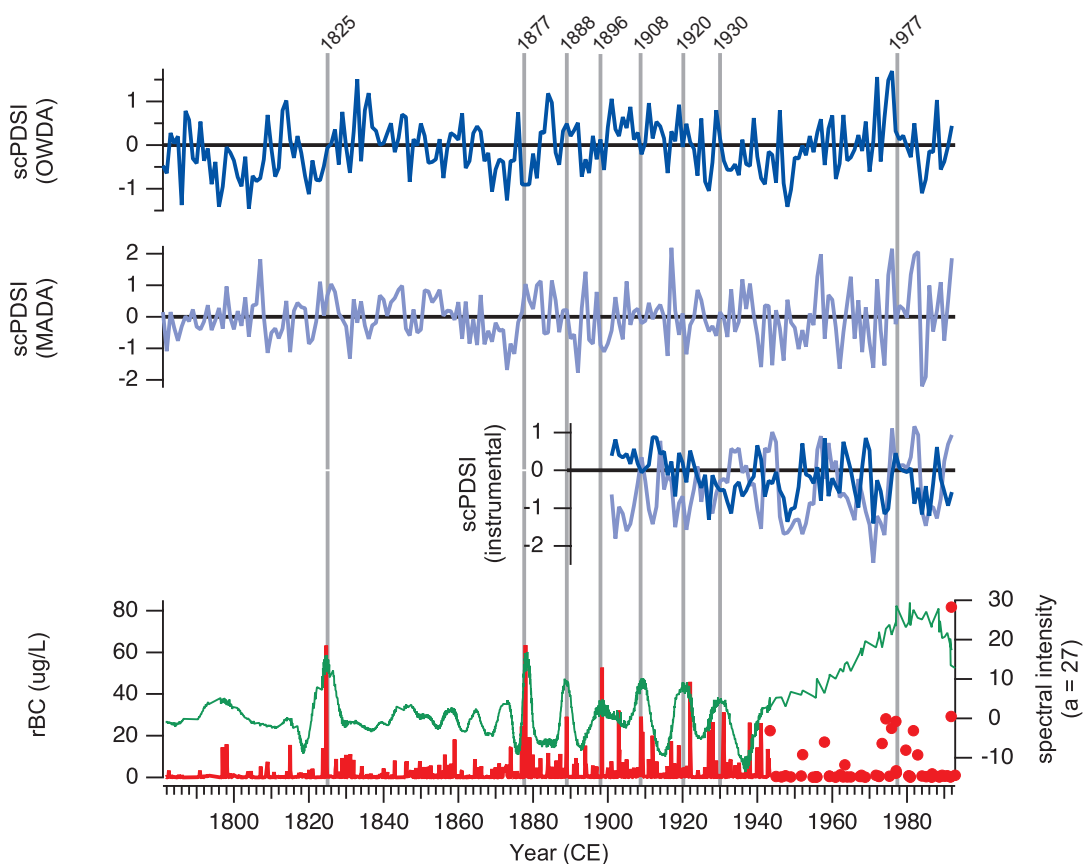
Source: © 2020 Google

975

976 Fig. 5: Frequency of back trajectories for airmasses arriving at the Mt. Xixiabangma a)
977 July, b) January. The area included in the Old World Drought Atlas (OWDA; Cook et al.,
978 2015) and the Monsoon Asia Drought Atlas (MADA; Cook et al., 2010) reconstructions
979 is indicated (c).
980



981 Figure 6:



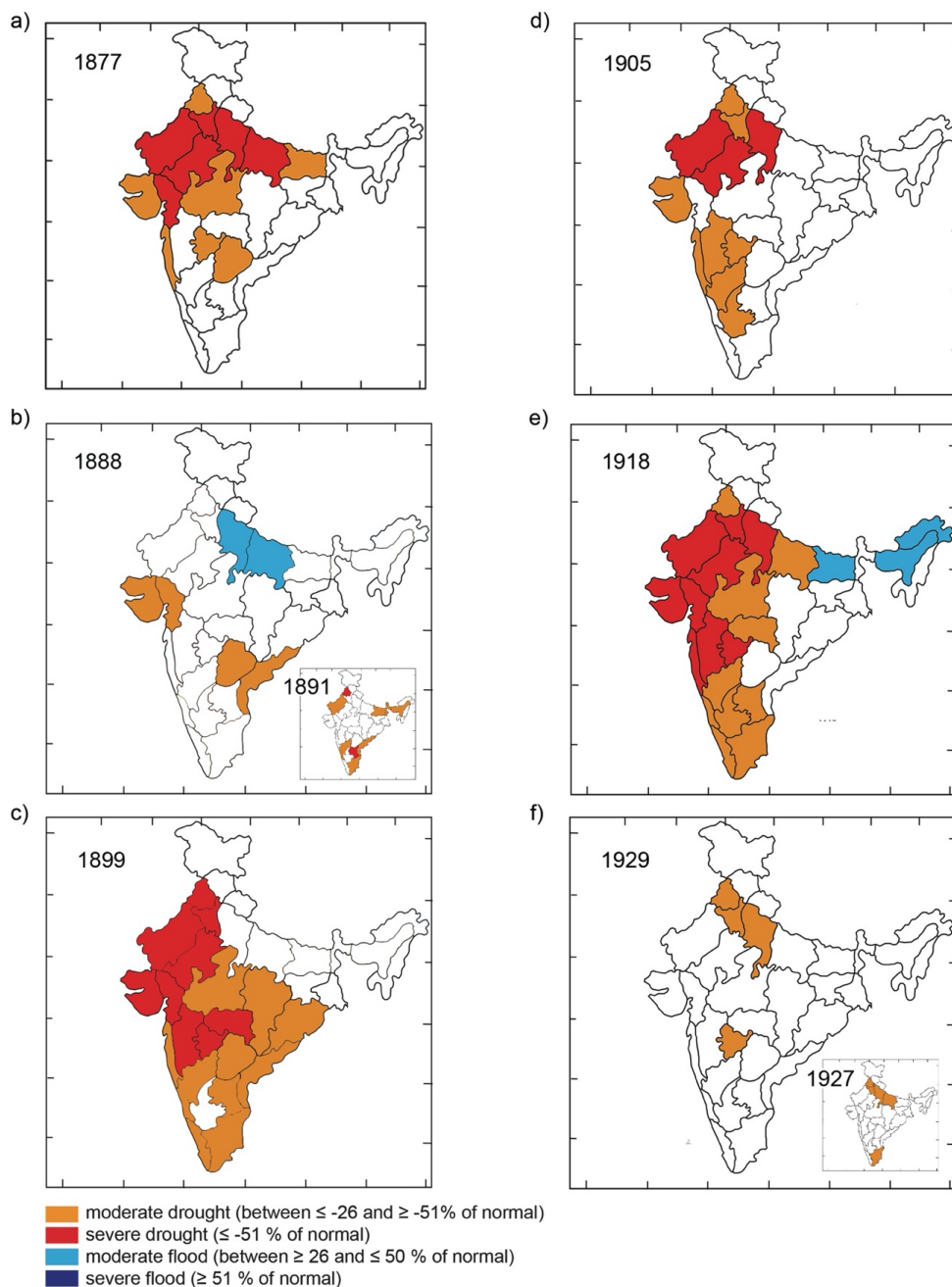
982

983 Fig. 6: The Dasuopu rBC record (in red) compared to regional reconstructed and
984 instrumental climate records from the Old World Drought Atlas (OWDA; dark blue) and
985 the Monsoon Asia Drought Atlas (MADA; light blue). Note the correspondence between
986 negative self-calibrating Palmer Drought Severity Index (scPDSI) and periods of high
987 rBC deposition. Data for both the reconstructed and instrumental climate records are
988 obtained from; OWDA (drought.memphis.edu/OWDA/) and MADA
989 (drought.memphis.edu/MADA/).

990



991 Figure 7:



992

993

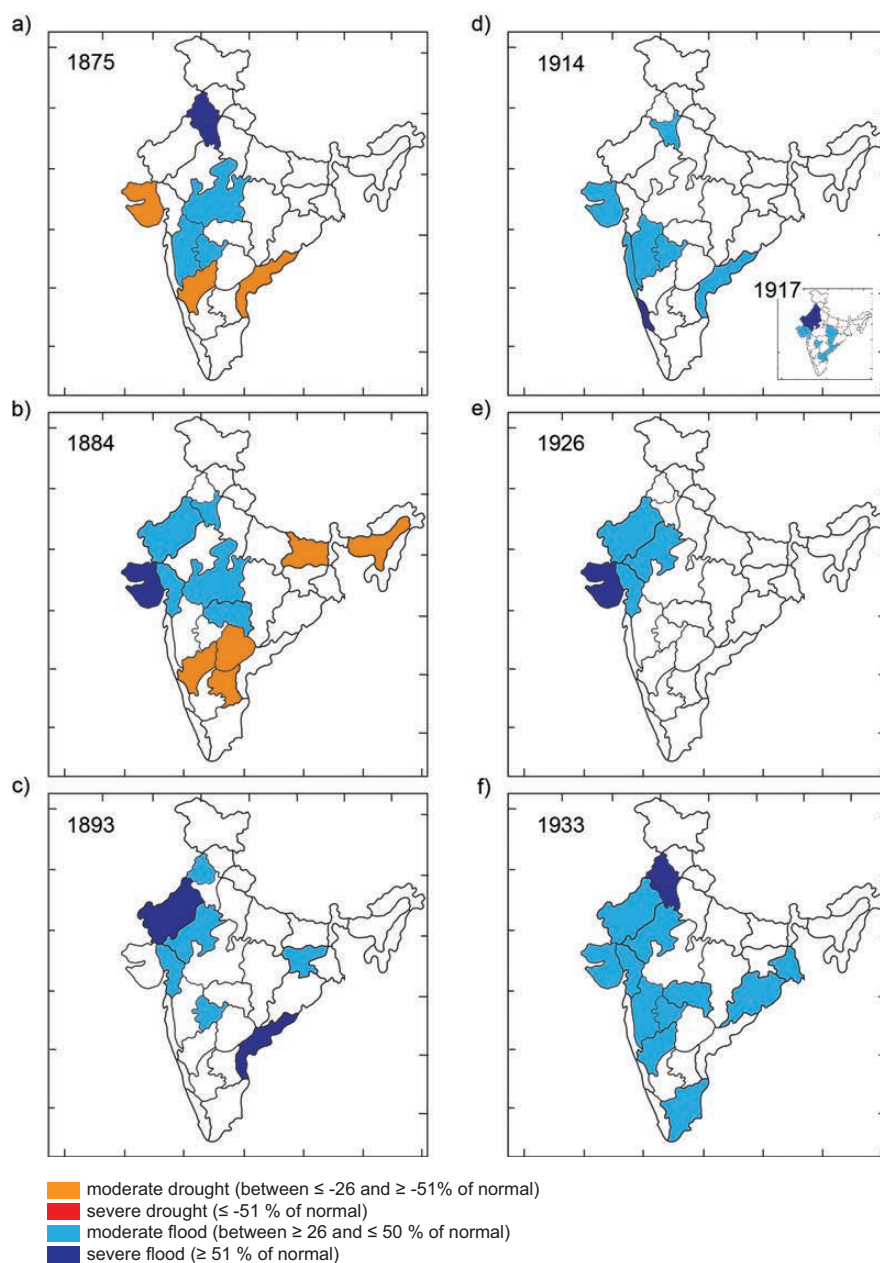
994

995

Fig. 7: The distribution of meteorologic subdivisions in NW India reporting drought during periods of high spectral intensity at a = 27 scale.



996 Figure 8:



997
998
999
1000
1001

Fig. 8: The distribution of meteorologic subdivisions in NW India reporting flood conditions during periods of low spectral intensity at a = 27 scale.



1002 Table 1:

trace element (ⁿ)	total <i>r_s</i>	pre-1877 <i>r_s</i>	post-1877 <i>r_s</i>	EF total <i>r_s</i>	EF pre-1877 <i>r_s</i>	EF post-1877 <i>r_s</i>
Al ⁽⁹¹⁵⁾	0.22	0.40	-0.08	-0.45	-0.40	-0.55
As ⁽⁹¹⁴⁾	0.23	0.41	-0.06	-0.41	-0.41	-0.44
Ba ⁽⁹¹⁶⁾	0.26	0.43	-0.07	-0.24	-0.25	-0.28
Bi ⁽⁸⁵⁷⁾	0.20	0.40	-0.10	-0.37	-0.33	-0.44
Cd ⁽⁹¹⁶⁾	0.23	0.37	-0.07	-0.5	-0.48	-0.62
Co ⁽⁹¹⁵⁾	0.23	0.41	-0.09	-0.38	-0.40	-0.42
Cr ⁽⁹¹⁵⁾	0.19	0.38	-0.09	-0.56	-0.53	-0.64
Cs ⁽⁹¹³⁾	0.25	0.41	-0.04	-0.39	-0.35	-0.48
Fe ⁽⁹¹⁵⁾	0.23	0.42	-0.07			
Ga ⁽⁹¹⁵⁾	0.22	0.39	-0.07	-0.57	-0.54	-0.68
Mg ⁽⁹¹⁵⁾	0.24	0.44	-0.09	-0.21	-0.20	-0.22
Mn ⁽⁹¹⁵⁾	0.24	0.44	-0.10	0.02	-0.01	0.06
Mo ⁽⁹¹⁵⁾	0.22	0.37	-0.08	-0.54	-0.52	-0.63
Nb ⁽⁹¹⁵⁾	0.21	0.36	-0.04	-0.48	-0.46	-0.59
Ni ⁽⁹¹⁵⁾	0.22	0.39	-0.09	-0.5	-0.50	-0.57
Pb ⁽⁹¹⁶⁾	0.23	0.40	-0.08	-0.31	-0.31	-0.35
Rb ⁽⁹¹⁴⁾	0.27	0.43	-0.05	-0.49	-0.47	-0.60
Sb ⁽⁹¹⁶⁾	0.19	0.38	-0.07	-0.56	-0.52	-0.65
Ti ⁽⁹¹⁴⁾	0.23	0.41	-0.08	-0.28	-0.25	-0.42
Tl ⁽⁹¹⁶⁾	0.24	0.42	-0.08	-0.52	-0.49	-0.62
U ⁽⁹¹⁶⁾	0.24	0.41	-0.07	-0.29	-0.29	-0.34
V ⁽⁹¹⁵⁾	0.24	0.40	-0.07	-0.52	-0.51	-0.63
Zn ⁽⁹¹⁵⁾	0.15	0.26	-0.06	-0.53	-0.52	-0.63

1003

1004 Table 1. The Spearman correlation coefficient (*r_s*, $\alpha=0.01$) for trace elements and the
 1005 trace element enrichment factor (EF) relative to rBC concentration throughout the
 1006 Dasuopu ice core. Italics indicate a non-statistically significant *r_s*.